JGR Biogeosciences

RESEARCH ARTICLE
10.1029/2024JG008615

Key Points:

- Variability of ^{17}O-excess in precipitation is small compared to that of phytoliths in response to RH change
- The triple oxygen isotope composition of water is a powerful tracer of evaporation and mixing in soil and plant waters
- The triple oxygen isotope composition of plant water can be used to trace the origin of water taken up by the plants

Correspondence to:
A. Alexandre,
alexandre@cerege.fr

Citation:
Alexandre, A., Outrequin, C., Vallet-Coulomb, C., Peugeot, C., Grippa, M., Aleman, J., et al. (2025). What does the triple isotopic composition of oxygen in precipitation, groundwater, soil water, plant water, and phytoliths reveal about current and past hydrological cycles? *Journal of Geophysical Research: Biogeosciences*, *130*, e2024JG008615. https://doi.org/10.1029/2024JG008615

Received 22 NOV 2024
Accepted 23 SEP 2025
Corrected 3 NOV 2025

This article was corrected on 3 NOV 2025. See the end of the full text for details.

Author Contributions:
Conceptualization: Anne Alexandre, Christine Vallet-Coulomb
Data curation: Anne Alexandre, Christophe Peugeot, Manuela Grippa, Eric Mougin
Formal analysis: Anne Alexandre, Clement Outrequin, Christine Vallet-Coulomb, Christophe Peugeot, Amaelle Landais, Eric Mougin
Funding acquisition: Anne Alexandre
Investigation: Anne Alexandre, Clement Outrequin, Christine Vallet-Coulomb, Manuela Grippa, Julie Aleman, Claudia Voigt, Amaelle Landais, Eric Mougin, Jérôme Ogée, Nogmana Soumaguel, Rasmus Fensholt

What Does the Triple Isotopic Composition of Oxygen in Precipitation, Groundwater, Soil Water, Plant Water, and Phytoliths Reveal About Current and Past Hydrological Cycles?

Anne Alexandre[1], Clement Outrequin[1], Christine Vallet-Coulomb[1], Christophe Peugeot[2], Manuela Grippa[3], Julie Aleman[1], Claudia Voigt[1,4], Amaelle Landais[5], Eric Mougin[3], Ousmane Ndiaye[6], Corinne Sonzogni[1], David Au Yang[1], Jean-Charles Mazur[1], Martine Couapel[1], Jérôme Ogée[7], Theodore Ouani[8], Simon Afouda[8], Maxime Wubda[8], Nogmana Soumaguel[9], Alfred Houngnon[10], Torbern Tagesson[11], and Rasmus Fensholt[12]

[1]Aix Marseille University, CNRS, IRD, INRA, Coll France, CEREGE, Aix-en-Provence, France, [2]Hydrosciences Montpellier, IRD, CNRS, University Montpellier, Montpellier, France, [3]Géosciences Environnement Toulouse, University Toulouse, CNRS, IRD, CNES, Toulouse, France, [4]Institute of Soil Sciences and Site Ecology, TU Dresden, Tharandt, Germany, [5]Laboratoire des Sciences du Climat et de l'Environnement (LSCE/IPSL/CEA/CNRS/UVSQ), Gif-sur-Yvette, France, [6]ISRA-Centre de Recherches Zootechniques, Dahra, Sénégal, [7]INRAE, Bordeaux Sciences Agro, UMR ISPA, Villenave-d'Ornon, France, [8]IRD Bénin, Cotonou, Bénin, [9]Centre IRD, Bamako, Mali, [10]AGIR, Association de Gestion Intégrée des Ressources, Cotonou, Bénin, [11]Department of Physical Geography and Ecosystem Sciences, Lund University, Sölvegatan, Sweden, [12]Department of Geosciences and Natural Resource Management, University of Copenhagen, Copenhagen, Denmark

Abstract Quantitative data are needed to constrain the feedback loops between vegetation and hydroclimate. In this study, the amplitudes of variations in the triple oxygen isotope composition of water at the soil-plant-atmosphere interface are measured in savanna and dry forest contexts in West Africa (Benin and Senegal). Comparison of in situ data and model estimates reveals the following: (a) The value of ^{17}O-excess for reconstructing climate archives is confirmed, given its small variability in precipitation (a few per meg) compared to the very large magnitude of change in the ^{17}O-excess of phytoliths (hundreds of per meg) in response to RH changes. (b) At the beginning of the dry season, the ^{17}O-excess in soil water is lower than that of precipitation by only 30 per meg in the sandy-loam soils and 50 per meg in the sandy soil. This shows the limited contribution of evaporated water to bulk soil water and provides clues to constrain the complex hydrological functioning of soils; (c) The regression line connecting the triple oxygen isotope composition of water in the stems and leaves of grasses and trees can be used to determine the origin of the water absorbed by the roots. Semi-evergreen trees draw their water from the water table during the dry season, whereas grasses and semi-evergreen trees use surface water during the wet season. These original data open up new perspectives for the use of the triple oxygen isotope composition of water and phytoliths to better understand current and past hydrological cycles.

Plain Language Summary In this study, we examine the triple oxygen isotope composition of water at the soil-plant-atmosphere interface and of plant silica (phytoliths), at three instrumented sites in West Africa (Senegal and Benin). By using in situ measurements and a simple mechanistic model, we show that the ^{17}O-excess, which is a new isotopic marker, varies little in annual precipitation, slightly more in soil water, and significantly in plant water and phytoliths, in link with changes in atmospheric relative humidity. This demonstrates the relevance of using the ^{17}O-excess of phytoliths for climate reconstructions. Our results additionally show that evaporation affects only a small portion of the water in the soil, even at the very beginning of the rainy season when atmospheric humidity is still low. Finally, we present how the triple isotopic composition of plant water (from grasses and trees) can provide information about the origin of water pumped by the roots: groundwater or surface water. The triple isotopic composition of oxygen is a powerful tool for understanding current and past water cycles.

1. Introduction

Interactions between vegetation and hydroclimate are difficult to properly account for in Earth System Models (ESMs), particularly in dry regions (Green et al., 2024; Zhang et al., 2022). Data to constrain these models, for

Methodology: Anne Alexandre, Christophe Peugeot, Manuela Grippa, Claudia Voigt, Amaelle Landais, Eric Mougin, Ousmane Ndiaye, Corinne Sonzogni, David Au Yang, Jean-Charles Mazur, Martine Couapel, Jérôme Ogée, Theodore Ouani, Simon Afouda, Nogmana Soumaguel, Alfred Houngnon
Project administration: Anne Alexandre, Christophe Peugeot
Resources: Anne Alexandre, Clement Outrequin, Christine Vallet-Coulomb, Christophe Peugeot, Manuela Grippa, Amaelle Landais, Eric Mougin, Ousmane Ndiaye, Rasmus Fensholt
Supervision: Anne Alexandre, Torbern Tagesson
Validation: Anne Alexandre, Christophe Peugeot
Visualization: Anne Alexandre, Torbern Tagesson
Writing – original draft: Anne Alexandre, Clement Outrequin, Christine Vallet-Coulomb, Christophe Peugeot, Manuela Grippa, Julie Aleman, Claudia Voigt, Amaelle Landais, Eric Mougin, Ousmane Ndiaye, Corinne Sonzogni, David Au Yang, Jean-Charles Mazur, Martine Couapel, Jérôme Ogée, Theodore Ouani, Simon Afouda, Nogmana Soumaguel, Alfred Houngnon, Torbern Tagesson, Rasmus Fensholt
Writing – review & editing: Anne Alexandre, Clement Outrequin, Christine Vallet-Coulomb, Christophe Peugeot, Manuela Grippa, Julie Aleman, Claudia Voigt, Amaelle Landais, Eric Mougin, Ousmane Ndiaye, Corinne Sonzogni, David Au Yang, Jean-Charles Mazur, Martine Couapel, Jérôme Ogée, Theodore Ouani, Simon Afouda, Nogmana Soumaguel, Alfred Houngnon, Torbern Tagesson, Rasmus Fensholt

the present and the past, are strongly needed. It is now possible to measure the triple oxygen isotopic composition of biogenic minerals and water with high precision, either by Isotope Ratio Mass Spectrometry (IRMS) or by Cavity Ring Down Spectrometry (CRDS) (Aron et al., 2020; Gázquez et al., 2018; Huth et al., 2022; Outrequin et al., 2021; Passey et al., 2014; Sha et al., 2023; Surma et al., 2021; Voigt et al., 2023; Xia et al., 2023). This opens up new perspectives for the study of present and past water cycles at the soil-plant-atmosphere interface.

The triple oxygen isotopic composition of water provides information on evaporation and mixing processes in the continental water cycle. The $\delta^{18}O$ and $\delta^{17}O$ of meteoric waters are related and usually align along the Global Meteoric Water Line (GMWL) expressed by (Equation 1; Terzer-Wassmuth et al., 2023):

$$\delta'^{17}O = 0.5280\ (\pm 0.0002) \times \delta'^{18}O + 0.0153\ (\pm 0.0013) \quad (1)$$

with

$$\delta'^{*}O = 1000 \times \ln(\delta/1000 + 1) \quad (2)$$

and

$$\delta^{*}O = \left({}^{*}O/{}^{16}O\right)_{sample}/\left({}^{*}O/{}^{16}O\right)_{standard} - 1 \text{ where } {}^{*} \text{ stands for 18 or 17.} \quad (3)$$

δ and δ' are expressed in ‰. The second order parameter ^{17}O-excess describes the deviation of $\delta'^{17}O$ from a reference line with the slope of the GMWL:

$$^{17}O\text{-excess} = \delta'^{17}O - 0.528 \times \delta'^{18}O \quad (4)$$

Because the variations of ^{17}O-excess in natural waters are rather small, it is expressed in per meg (10^{-6}). The ^{17}O-excess can be compared to the d-excess, the second order parameter in the $\delta^{2}H$ versus $\delta^{18}O$ system, commonly used in hydrological studies and expressed in ‰:

$$d - \text{excess} = \delta^{2}H - 8 \times \delta^{18}O \quad (5)$$

with

$$\delta D = \left({}^{2}H/{}^{1}H\right)_{sample}/\left({}^{2}H/{}^{1}H\right)_{standard} - 1 \quad (6)$$

The fractionation factor α between a and b follows:

$$\alpha^{17}O_{a-b} = \left(\alpha^{18}O_{a-b}\right)^{\theta a-b} \quad (7)$$

which can also be expressed as:

$$\theta_{a-b} = \ln \alpha^{17}O_{a-b}/\ln \alpha^{18}O_{a-b} \quad (8)$$

In contrast to θ_{a-b} which is linked to a particular physical process (equilibrium or kinetic), λ_{a-b} is empirically measured between two groups of materials and may not be related to a single process. It is expressed as:

$$\lambda_{a-b} = \left(\delta'^{17}O_a - \delta'^{17}O_b\right)/\left(\delta'^{18}O_a - \delta'^{18}O_b\right) \quad (9)$$

in the $\delta'^{18}O$ versus $\delta'^{17}O$ space.

Evaporation determines the ^{17}O-excess of water via three fractionating mechanisms, conceptualized by the Craig and Gordon model (Figure 1a) (Barkan & Luz, 2007; Craig & Gordon, 1965). The ^{17}O-excess of residual water decreases with the residual fraction of evaporated water. The impact is higher the lower relative humidity (RH) (Figure 1b). Mixing between waters of different isotopic composition additionally drives the ^{17}O-excess of water (Voigt et al., 2021) (Figure 1c). In the ^{17}O-excess versus δ'^{18}O system, evaporation, and mixing produce two clearly distinct curves, whereas in the d-excess versus δ^{18}O system, the two curves are indistinguishable. This is one of the main advantages of the triple oxygen isotopic system for tracing processes in the water cycle. Another advantage over d-excess is that ^{17}O-excess is insensitive to equilibrium fractionation and water phase changes.

Among terrestrial surface waters, leaf water shows the greatest variations in ^{17}O-excess (ca. 150 per meg) (Alexandre et al., 2019; Landais et al., 2006; Li et al., 2017; Outrequin et al., 2021; Voigt et al., 2023). It responds to rapid changes in RH due to the small size of the water reservoir represented by the leaf and the small contribution of unevaporated water circulating in the leaf veins. In precipitation, the few long term records published to date show that ^{17}O-excess varies much less than in leaf water on an event or monthly scale (ca. 70 per meg) and even less than analytical precision (5–10 per meg) on an interannual scale (Aron et al., 2021; He et al., 2021; Kaseke et al., 2018; Liang et al., 2024). This is due to its insensitivity to equilibrium fractionation and water phase changes. Unlike precipitation and plant water, the triple oxygen isotopic composition of soil water has so far received little attention. The only study to date (Beverly et al., 2021) shows that despite highly evaporative conditions, the difference in ^{17}O-excess between precipitation and bulk soil water is limited (<50 per meg if abnormally high ^{17}O-excess values are not considered). This is much less than the difference between precipitation and soil water at the evaporative front, estimated at about 150–200 per meg using a simple steady state model (Kelson et al., 2023).

The first objective of this study is to complement the above-mentioned studies (Alexandre et al., 2019; Aron et al., 2021; Beverly et al., 2021; He et al., 2021; Kaseke et al., 2018; Landais et al., 2006; Li et al., 2017; Liang et al., 2024; Outrequin et al., 2021) and test the potential of the triple oxygen isotopic composition in water to characterize exchanges and mixings in the water cycle at the soil-plant-atmosphere interface. For this purpose, we setup a monitoring of the triple oxygen isotopic composition of precipitation, groundwater, soil, and plant water at three instrumented sites in West Africa (Benin and Senegal), where climate and vegetation have been measured for several years.

Understanding the evolution of the triple oxygen isotopes in the present-day water cycle is essential for studying past hydroclimates. Unlike d-excess, ^{17}O-excess can be analyzed in biogenic and authigenic fossil minerals preserved in geological archives. One of them is amorphous silica that polymerizes in or between plant cells under the form of phytoliths. In the triple oxygen isotopic system, a constant apparent fractionation between leaf water and phytolith ($\lambda_{\text{phyto-water}}$) has been demonstrated (Alexandre et al., 2018, 2019; Outrequin et al., 2021). Additionally, a direct relationship between the ^{17}O-excess of phytoliths ($^{17}\text{O-excess}_{\text{phyto}}$) and RH was calibrated in growth chamber for the RH range 40%–80% (Outrequin et al., 2021):

$$\text{RH}\ (\%) = 0.21\ (\pm 0.02) \times {}^{17}\text{O-excess}_{\text{phyto}}\ (\text{per meg}) + 112\ (\pm 6) \quad (10)$$

Testing whether this relationship is also valid in natural settings is a prerequisite to reconstruct past changes in RH over continents (Guo et al., 2025). Having a quantitative RH proxy on hand would be a major breakthrough as RH is a crucial climate variable to consider when investigating the response of terrestrial ecosystems to climate change. It is the driving force of surface water evaporation and thus impacts the hydrological balance of lakes. It also drives soil evaporation, hence soil moisture, and the Vapor Pressure Deficit (VPD, a combination of temperature and RH). Both soil moisture and VPD drive plant transpiration, photosynthesis and productivity through their influence on stomatal conductance (Grossiord et al., 2020; Liu et al., 2020; López et al., 2021). Although the $^{17}\text{O-excess}_{\text{phyto}}$ holds promise as a proxy for RH, it still requires further calibration to enable accurate regional reconstructions. These quantitative reconstructions are necessary for investigating feedbacks between vegetation and RH and for model-data comparisons. Taking advantage of the water isotopic monitoring (objective 1) and previous calibrations (Equation 10), the second objective of this study is to specify which RH signal is recorded by grass $^{17}\text{O-excess}_{\text{phyto}}$ at the monitored West African sites: RH averaged over the year or over the rainy season, during diurnal or whole day periods? Answering these questions is critical to improve the accuracy and interpretability of this new RH proxy.

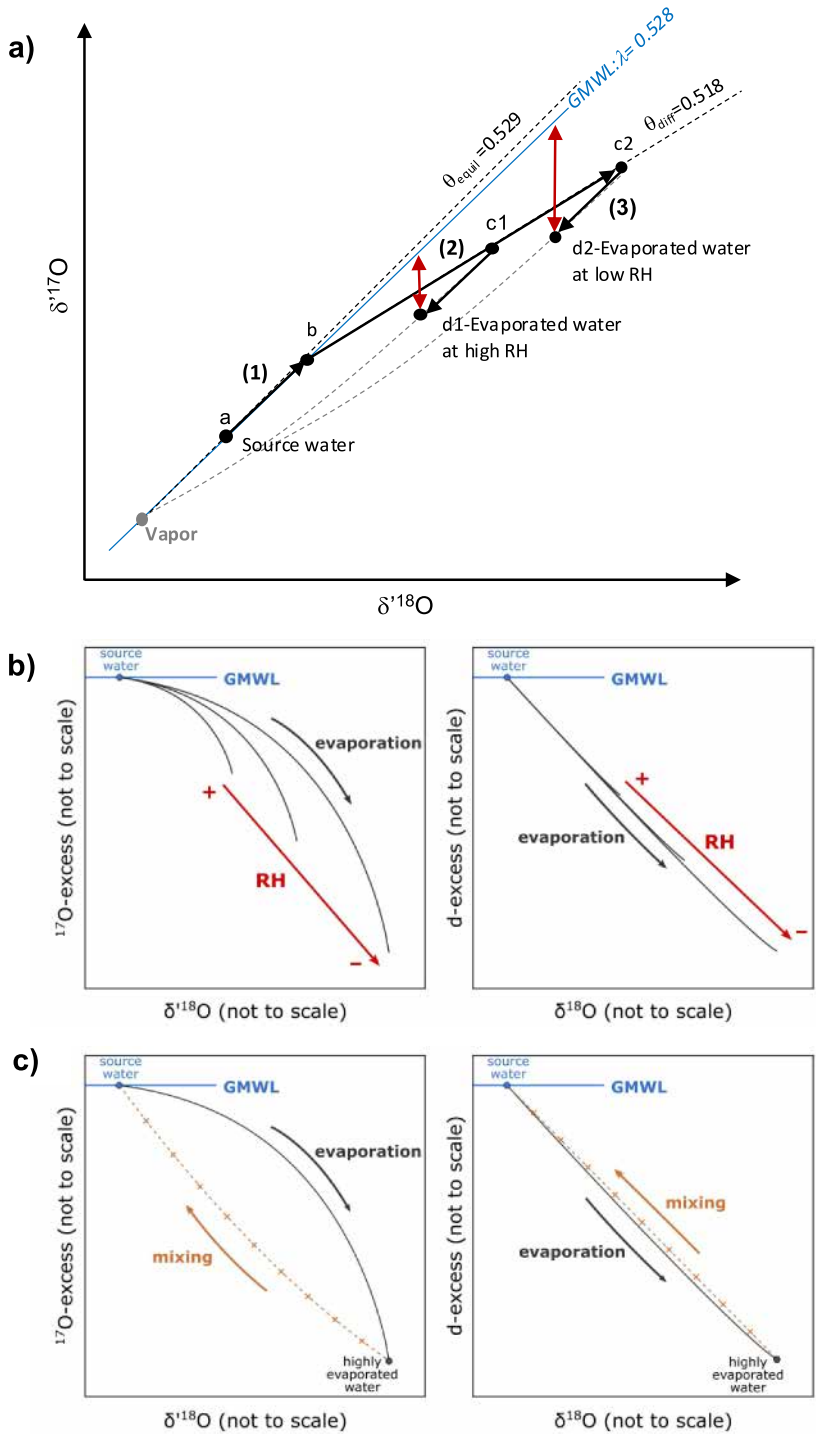

Figure 1. (a) Schematical representation of the three fractionating mechanisms that interact during water evaporation, as conceptualized by the Craig and Gordon model: (1) from (a) to (b) equilibrium fractionation between source water (unevaporated) and saturated atmospheric vapor layer; (2) from (b) to (c1 or c2): fractionation due to water vapor diffusion from the saturated layer to humid (c1) or dry air (c2); (3) from (c) to (d) fractionation due to exchange between evaporated water and atmospheric water vapor at high (c1–d1) and low (c2–d2) relative humidity (RH). Red arrows: magnitude of the resulting ^{17}O-excess. θ_{equil} (0.529): equilibrium fractionation in the triple oxygen isotopic system (Barkan & Luz, 2005), here equivalent to the slope of the equilibrium line; θ_{diff} (0.518): diffusion fractionation (Barkan & Luz, 2007), here equivalent to the slope of the diffusion line. Note that since the value of 0.528, considered in the ^{17}O-excess calculation, is close to θ_{equil} (0.529), the ^{17}O-excess of water depends little on equilibrium fractionation processes and is very suitable for quantifying evaporative kinetic fractionation that is RH-dependent. (b) Evolution of the ^{17}O-excess versus δ'^{18}O of an evaporated water as a function of the evaporated fraction for decreasing RH (Craig & Gordon, 1965 or eq. 14 in Gonfiantini et al., 2018). (c) Evolution of the ^{17}O-excess and δ'^{18}O of a mixture between unevaporated and evaporated water pools (Equation 14 in Gonfiantini et al., 2018 and mixing equation). Crosses represent the proportion of evaporated water.

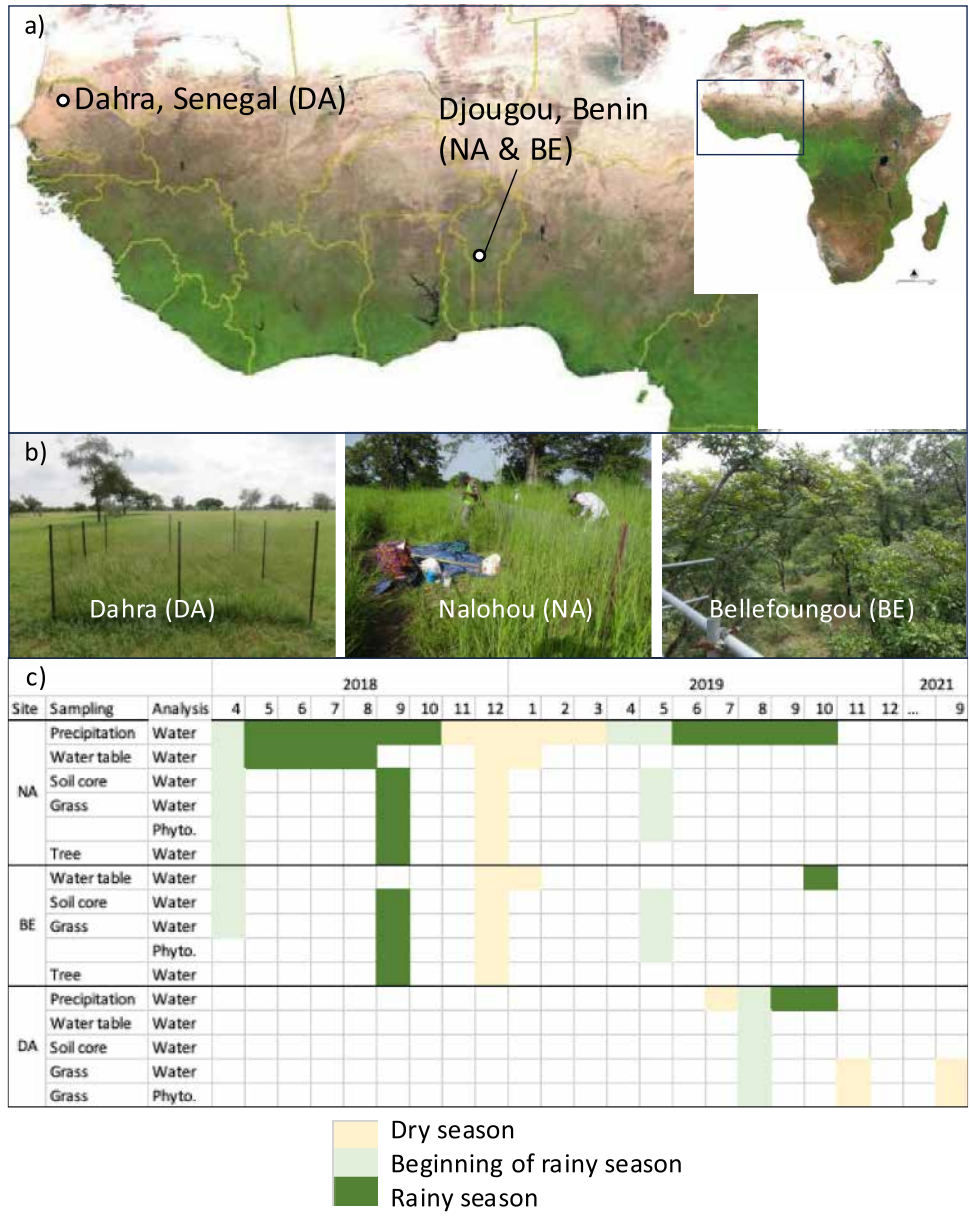

Figure 2. (a) Location of the AMMA-CATCH sites in Benin and Senegal on a SPOT 4—derived land-cover map of Africa (Mayaux et al., 2004). Nalohou (NA) and Belefoungou (BE) sites are located in the sub-humid ecoclimatic zone of Benin, 13 km from each other, close to the town of Djougou. The site of Dahra (DA) is located in the Sahelian zone, at the Center for Zootechnical Research in Dahra, Senegal. (b) Pictures of vegetation during rainy season at the 3 studied sites: sub-humid tall grass savanna at NA, dry forest at BE, Sahelian tree and shrub short grass savanna at DA. (c) Sampling and type of sample analyzed according to site, year, month and dry or rainy season. Details of sampling are given in Alexandre (2025).

2. Materials and Methods

2.1. Study Sites

The three study sites are part of the long-term eco-hydro-meteorological observatory for West Africa AMMA-CATCH (Multidisciplinary Analysis of the African Monsoon—Coupling the Tropical Atmosphere and the Hydrological Cycle) (AMMA-CATCH, 2024; Galle et al., 2018).

The Nalohou (NA) and Belefoungou (BE) sites (Figure 2; Table 1) are located in the sub-humid ecoclimatic zone of Benin. The climate has a 5-month dry season. At BE, the soil is ferruginous with sandy-loamy horizons and

Journal of Geophysical Research: Biogeosciences

10.1029/2024JG008615

Table 1
Location of the AMMA-CATCH Sites in Belefoungou (BE, Benin), Nalohou (NA, Benin), and Dahra (DA, Senegal)

										Annual							Grass growth season						
											Daily			Diurnal			Daily			Diurnal			
Site		Lat. N	Long. E	Vegetation type	Dominant grass species	Dominant tree species	Soil	Climate	Rainy season	Precipitation mm/yr	T_{air} °C	RH_2 %	RH_{15}	T_{air} °C	RH_2 %	RH_{15}	T_{air} °C	RH_2 %	RH_{15}	T_{air} °C	RH_2 %	RH_{15}	Years
BENIN	Bellefoungou (BE)	9°44′	1°36′	Dry forest, canopy at 15 m on average	Perennial	Semi-evergreen	Tropical ferrugineous on lateritic crust Sandy-loamy	Sub-humid	Apr –Oct	1,339	25.8 (2 m) 26.2 (15 m)	65.7 (5 m)	56.3	28.3 (2 m) 27.9 (15 m)	58.9 (5 m)	51.4	26.0 (5 m) 26.0 (15 m)	80.7 (5 m)	72.7	27.7 (2 m) 27.3 (15 m)	73.9 (2 m)	67.2	2017–2019
	Nalohou (NA)	9°47′	1°42′	Tall grass savanna						1,573	25.4	57.3	–	27.6	51.5	–	25.3	71.0	-	26.8	65.6	–	2018–2021
SENEGAL	Dahra (DA)	15°20′	15°26′	Tree and shrub short grass savanna	Annual	Continuous leafing and semi-deciduous	Tropical subarid isohumic on fixed sandy dunes Sandy	Semi-arid	Aug –Sept.	370	28.7	37.7		31	32.4		28.7	57.5	30.7	50.6			

Note. Soil, vegetation and climate averages are presented. Climate parameters were measured on site during the monitoring. RH was measured at 2 m height (RH_2) at the three sites and at 5 and 15 m height (RH_{15}) at BE. The grass growth season coincides with the rainy season at the three sites. Raw data are available in Alexandre (2025).

lateritic crust residues. A water table is located between 5 and 18 m depth (Herzog et al., 2021). The area is covered by a dry semi-deciduous forest resulting from the degradation of a forest dominated by leguminous plants. The leaf area index is between 0.5 and 3.5 m^2 m^{-2} throughout the year (Mamadou et al., 2016). The tree dominant species (*Isoberlinia doka*, *Isoberlinia tomentosa,* and *Pericopsis laxiflora)* are semi-evergreen, indicating only short-term water resource limitation. The average height of the tree is 8 m but individuals can reach 35 m. The grass species, dominated by *Andropogon gayanus* and *Imperata cylindrica* are perennial. They start growing at the beginning of the rainy season, and enter senescence shortly after rain stops, and soil moisture reaches the permanent wilting point. The grasses are never taller than 1 m height due to the tree competition for light (Awessou et al., 2017; Leroux et al., 2016; Seghieri et al., 2009). At NA, 13 km from BE as the crow flies, the soil is similar to the one in BE, except that a perched, seasonal water table is present close to the surface, generally between 1.5 and 3 m depth (Hector et al., 2015, 2018). The site is a former fallow land subject to annual controlled fires and vegetation is dominated by sub-humid savanna plant species. The total Leaf Area Index (LAI), including grasses and trees, ranges between 0.25 and 3 m^2 m^{-2} (Mamadou et al., 2016). Trees are semi-evergreen and dominated by *Vitellaria paradoxa* and *Parkia biglobosa* (Seghieri et al., 2009). The herbaceous stratum is dominated by the perennial *Andropogon gayanus* and the annual *Hyparrhenia involucrata* that can reach 2.5 m height during the rainy season (Awessou et al., 2017; Leroux et al., 2016; Seghieri et al., 2009). As for BE, the growth season for these herbaceous plants closely coincides with the rainy season, that is, from April–May to September–October.

The Dahra (DA) site (Figure 2; Table 1) is located in the Sahelian zone in Senegal, at the Center for Zootechnical Research in Dahra, Senegal. The climate is semi-arid with a long dry season and a short rainy season of approximately 3 months. The soil type is tropical subarid isohumic, developed on fixed sandy dunes. The vegetation is typical of a Sahelian woody savanna with a mix of trees shrubs and herbaceous species almost exclusively composed of annual plants and dominated by grasses. The maximum LAI of the herbaceous cover is approximately 2.5 m^2 m^{-2} (Fensholt et al., 2004). Shrubs and low trees are scattered (Tagesson et al., 2015) with a stock density of approximately 81 stems ha^{-1} and a canopy cover of ca. 6.8% (Agbohessou et al., 2023). Similarly to the southern sites in Benin, the growth period of these annual grasses closely coincides with the short rainy season, that is, from June to September.

2.2. Climate Monitoring and Rainwater Sampling

The three sites are equipped with meteorological stations. Precipitation amount, mean air temperature (T_{air}) and RH were measured at 15-min intervals at 2 m height. RH was additionally measured at 5, 15, and 18 m height at BE (below and above the forest canopy). Rainwater was sampled in collectors preventing evaporation (Gröning et al., 2012) after each major precipitation event, in 2018 and 2019 at NA and in 2019 at DA (Figure 2). Rainwater was not sampled at BE.

2.3. Plant and Soil Sampling

At each site, one or two 4 m^2 sampling plots were fenced to protect them from prescribed fire and grazing. The sampling campaigns took place during the rainy and dry seasons in 2018 and 2019 for NA and BE and in 2019 and 2021 for DA (Figure 2).

For water analysis, grass stems and leaves as well as new wood and leaves from trees were collected separately in NA and BE. In DA, the first grass shoots (with first leaves and little stem) were collected at the beginning of the rainy season. All collections took place at midday. Four grams of fresh material were immediately inserted into glass gastight vials. Wood and leaf were sampled from the dominant tree species close to the plots.

For phytolith analysis, grass stem, sheath and leaf samples (in BE and NA), or whole grasses (in DA), were collected in the plots during the campaigns and stored in dry conditions. The sheaths bear stomata and constitute the starting point for the isotopic enrichment of leaf water due to evaporation (Alexandre et al., 2019; Webb & Longstaffe, 2002). The respective biomass of sheaths, leaves and stems, at the BE and NA sites, were measured by weighing five samples of whole grass tussocks, either growing or having reached senescence after full growth.

About 30 soil cores ranging from 30 to 210 cm in length were taken inside or close to the plots using a multi-stage sludge sampler (AMS Inc. American Falls) containing 6 cm-high tubes, hermetically sealed after each coring operation.

2.4. Water Extraction and Triple Oxygen Isotopic Analyses

Bulk soil water is composed of water pools with different residence time, which have followed different vertical and lateral paths through different pore sizes (Sprenger & Allen, 2020; Sprenger et al., 2016). Extraction of these pools depends on the technique used; each of them having their pros and cons (Di Bonito et al., 2008; Orlowski et al., 2016). Here, centrifugation extraction was performed at CEREGE on all the cores sampled at BE, NA, and DA. Twenty g of bulk soil was introduced in 15–50 ml Amicon centrifugation tubes with 10 KDa molecular weight cutoff filter and centrifuged at 10,000 rpm (equivalent to 12,500 RCF xg) and 25°C for 30 min in a Jouan BR4i centrifuge at CEREGE. The proportion of water extracted was related to the total soil water quantified after heating at 120°C for 24hr. For comparison, cryogenic vacuum distillation was performed on two core sections from NA and DA, at ISPA, according to the procedure described in Barbeta et al. (2020).

Soil water, precipitation and groundwater samples were analyzed using a Picarro L2140-i wavelength-scanned cavity ring-down spectrometer (CRDS, California, USA) operated in ^{17}O-excess/high precision mode at CEREGE. Samples were systematically filtered at 0.45 µm prior to analysis. For the soils, the still colored solutions (after centrifugation filtration) were re-filtered with 0.2 µm paper filters. Each measurement run included two groups of three working standards for VSMOW-SLAP normalization, and three replicates of an additional working standard for long term quality assurance (QA, prepared from unfiltered tapwater). Eight injections were made from each sample vial and QA. A correction for memory effect was applied following Vallet-Coulomb et al. (2021), and the two first injections of each vial were systematically discarded. The long-term precision on the QA measurement was 0.032‰ for δ^{18}O, 0.020‰ for δ^{17}O, 0.34 ‰ for δD and 6 per meg for ^{17}O-excess (1 SD; n = 39 measurement runs). The average difference from the reference composition of the QA was 0.020, 0.011, 0.12 ‰ and 1 per meg, for δ^{18}O, δ^{17}O, δD and ^{17}O-excess, respectively. For precipitation, groundwater and DA soil water, three replicates were analyzed, on which the mean and SD were calculated. For BE and NA soil water, as the samples were very small, only one analysis was possible. The mean and SD were calculated over the six injections making up the analysis. No abnormally high values of ^{17}O-excess were observed in precipitation or soil water, as might be expected in the case of large spectral interference from organic volatiles. However we cannot rule out small offsets for soil waters (e.g., 40 per meg; Hutchings & Konecky, 2023).

Plant water was extracted by vacuum distillation and activated charcoal was used to remove volatiles. To achieve high precision, plant water was converted to O_2 using a fluorination line and then analyzed by dual-inlet isotope-ratio mass spectrometry (IRMS) (ThermoQuest Finnigan MAT 253 mass spectrometer) at LSCE, following established protocols (Landais et al., 2006). The measurement of each O_2 sample was performed through a sequence of 2 runs of 24 dual-inlet measurements. The overall precision associated with the measurements of plant water isotopic composition is calculated as the pooled SD for each water sample, each being processed at least twice on the fluorination line and then on the IRMS. It results in uncertainties of 0.1‰ for δ^{18}O and δ^{17}O and 6 per meg for ^{17}O-excess. δD was not measured.

All water isotopic compositions were normalized on the Vienna Standard Mean Ocean Water—Standard Light Antarctic Precipitation (VSMOW-SLAP) scale, with an assigned SLAP ^{17}O-excess value of zero, following the recommendations of Schoenemann et al. (2013). A comparison between CRDS (at CEREGE) and IRMS (at LSCE) water measurements of three laboratory standards was carried out during the analysis session. This comparison was previously published in Outrequin et al. (2021; Appendix B) where another plant water data set was presented. The differences were lower than 0.2 ‰, 0.1 ‰ and 10 per meg for δ^{18}O, δ^{17}O and ^{17}O-excess, respectively.

Comparison of the isotopic compositions of soil water obtained by centrifugation and by cryogenic distillation shows that the percentage of water extracted is close to 100% when using cryogenic distillation (Figure 3). In contrast, centrifugation extracts 60%–100% of water when applied to sandy soil (DA) and less than 60% of water when applied to sandy-loamy soil (NA). This suggests that centrifugation extract water circulating in coarse pores while distillation extract the bulk water circulating in coarse and fine pores. Both technics produce similar isotopic profiles with depth, which contradicts a significant biases in the ^{17}O-excess of soil water, due to the presence of volatiles. Centrifuged water is enriched in ^{18}O by a maximum of 1.5 ‰ compared to distilled water. ^{17}O-excess and d-excess are similar given the precision ranges, except for one depth. This shows that under the study conditions, water circulating in fine and coarse pores have close isotopic compositions.

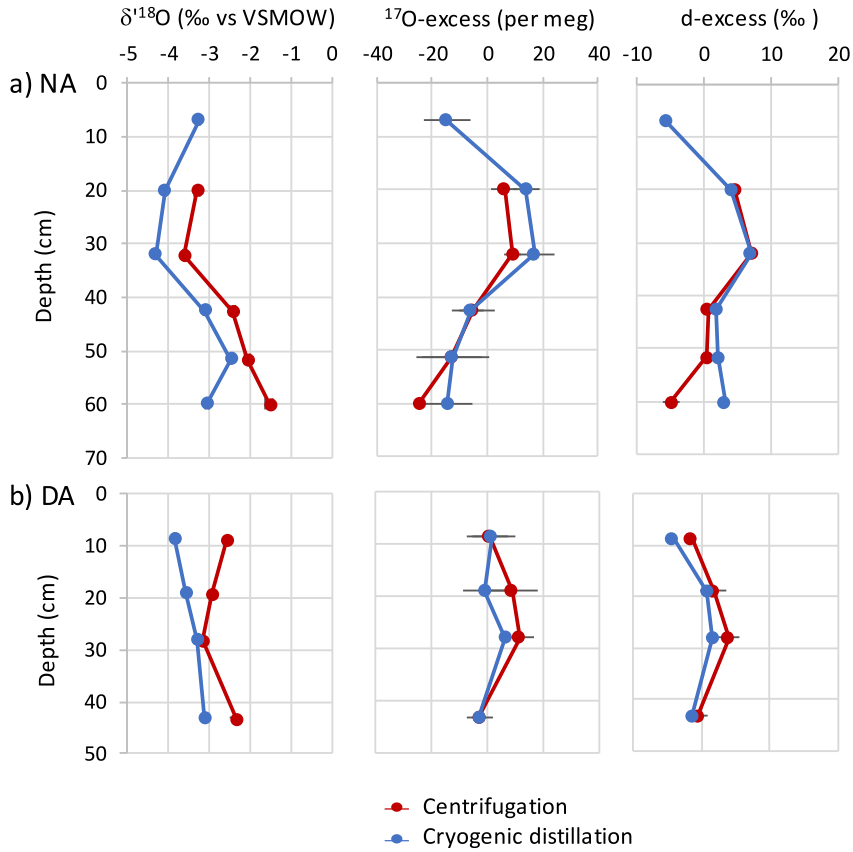

Figure 3. $\delta'^{18}O$, ^{17}O-excess and d-excess of soil water extracted by centrifugation and cryogenic distillation from a sandy-loamy soil core section collected at Nalohou, Benin (NA-P1-180519) and a sandy soil core section collected at Dahra, Senegal (DA-P1-240819). Error bars are not shown when they are smaller than the symbol. Data are available in Alexandre (2025).

2.5. Craig and Gordon Modeling

A model-data approach was used to interpret the observed isotopic composition of soil and plant waters. For soil water, we used the Craig and Gordon model applied to an isolated volume of water, to which a mixing equation between evaporated and non-evaporated water pools was added (Voigt et al., 2021). The last important precipitation before sampling was considered as the initial water from which evaporation can start. Climatic conditions prevailing at the time of sampling were used. For RH and T_{air}, the diurnal averages of the day of sampling were considered. Pure molecular diffusion (wind coefficient of 1) was assumed. For plant water, the Craig and Gordon model applied to leaf water (Equation 4 from Cernusak et al., 2016) that calculates the isotopic enrichment due to evaporation, was combined with a mixing equation that considers for grass leaves a 0.2 contribution (in volume) of unevaporated water circulating in the veins (Hirl et al., 2019; Outrequin et al., 2021; Voigt et al., 2023). For tree leaves, no significant contribution was assumed. For NA and DA grasses, precipitation preceding the sampling was taken as the initial water. For grasses from BE, where no precipitation was collected, the isotopic composition of precipitation at NA was considered as initial water. For trees from BE and NA the stem water was considered as the initial water. T_{leaf} was supposed to be 2°C lower than T_{air} (Voigt et al., 2023). The isotopic composition of atmospheric water vapor was considered in equilibrium with the precipitation water preceding the sampling. The diffusivity parameters considered were those from Merlivat (1978) and Luz et al. (2009).

2.6. Phytolith Extraction and Triple Oxygen Isotopic Analyses

Prior to extraction, plant samples were washed to remove particles that adhere to the surface stems and leaves via multiple baths in 1N HCl solution. Phytoliths were chemically extracted from plants and soils (Corbineau

et al., 2013; Crespin et al., 2008). Heavy liquid separation was performed for all soil samples and some plant samples to remove soil minerals other than amorphous silica. Purified phytoliths were weighted and concentrations reported as dry weight (d.w.) of bulk plant or soil matter. Purity of phytolith extracts was checked using polarized microscopy at a X600 magnification.

Phytolith extracts (1.6 mg) were dehydrated under a flow of $N_{2\ at\ 1100°C}$ to prevent the formation of siloxane from silanol groups during dehydroxylation. Molecular O_2 was extracted using the IR Laser-Heating Fluorination Technique (Alexandre et al., 2006; Crespin et al., 2008; Suavet et al., 2010). At the end of the procedure, the gas was passed through a −114°C slush to refreeze any molecule interfering with the mass 33 (e.g., NF potentially remaining in the line). The gas was directly sent to the dual-inlet mass spectrometer (ThermoQuest Finnigan Delta V Plus). Each gas sample was run twice. Each run consisted of eight dual inlet cycles (integration time of 26 s). A third run was performed when the standard deviation (s.d.) on the first two averages was higher than 15 per meg for ^{17}O-excess. The reproducibility from measurements of the quartz laboratory standard was 0.20 and 0.10 ‰ for δ^{18}O and δ^{17}O, respectively, and 9 per meg for ^{17}O-excess (1 s.d., n = 59). For the phytolith samples, the reproducibility on ^{17}O-excess was mostly lower than 15 per meg, always lower than 20 per meg (1 s.d., 2 to 3 aliquots).

The triple oxygen isotopic composition of silicates is expressed on the Vienna Standard Mean Ocean Water-*Standard Light Antarctic Precipitation* (VSMOW-SLAP) scale as recommended by Wostbrock and Sharp (2021). The sample measurements were corrected on a daily basis using a quartz laboratory standard analyzed at the beginning of the day until a ^{17}O-excess plateau was reached, and again in the middle and at the end of the day. The composition of the reference gas was determined against NBS28 (δ^{18}O = 9.570 ‰; δ^{17}O = 4.991 ‰; ^{17}O-excess = −50 per meg), on the basis of an interlaboratory comparison previsouly published (Appendix C in Outrequin et al., 2021).

2.7. Climate Data Processed for Grass Phytolith Production

At the three sites, daily (24hr) and diurnal totals (for precipitation) and averages (for RH and T_{air}) were compiled from one year before the first sampling to the end of the year of the last sampling (i.e., 2017–2019 at BE and NA, 2018–2021 at DA). Diurnal periods could vary between days and was based on measured incoming short wave radiation at the site to best match the time of the day when photosynthesis and transpiration take place. Gaps in RH and T_{air} (from a few days to 1 month) were filled using linear regression obtained from the record of the nearest AMMA-CATCH weather station. In the absence of a nearby record (e.g., at DA), gaps were filled by linear or spline interpolation over time on a moving average of the variable to be filled, to restore temporal dynamics. Precipitation totals and averaged RH and T_{air} were then calculated on an annual scale (Table 1) and for the growth period of the grasses sampled for phytolith extraction. These growth periods were defined on precipitation data as follows. At BE and NA sub-humid sites, the perennial grasses start their growth before the first rains, possibly triggered by the increase in RH. In a first approximation, we considered that the growth period of the perennials matched the rainy season, defined here from the first rainy day to the last rainy day preceding a dry month. A day was considered a rainy day if precipitation totals exceeded 2 mm. At DA semi-arid site, the annual grasses start their growth when there is enough soil water for their seeds to germinate while the end of their growth is controlled by photoperiod and soil drying, and occurs between mid- to end- September. The growth season is thus approximated from the first day with precipitation ≥10 mm to the last day with precipitation ≥2 mm preceding a dry month (in agreement with germination and senescence field observations).

The climate averages were weighted according to phytolith production. Grass biomass is assumed to increase steadily over the growing season (Fournier, 1991). Indeed, phytolith concentrations obtained from the grasses sampled at different growth stages suggested that the silicification rate increased linearly from the beginning to the end of the growth. Hence, the weighted average of a climate parameter (X_{Av}) was approximated as:

$$X_{Av} = \Sigma(N_i \times X_i) / \Sigma N_i \quad (11)$$

where N_i represents the growing day number (with 1 for the first rainy day of the growth period and i the end-of-growth day) and X_i is the averaged value of the climatic parameter X calculated for the growing period.

3. Results

3.1. Climate Conditions

The climate conditions, averaged over 2017–2019 in NA, and BE, and over 2018–2021 in DA, differ between the three sites, with mean annual precipitation ranging from 1,573 mm at NA to 370 mm at DA (Table 1). Interestingly, it has rained 234 mm less at BE than at NA although the two sites are ony 13 km apart. Annual daily RH measured at 2 m height is only 38% at DA, whereas it reaches 56%–57% at NA and even 66% at BE (below the canopy). At BE, RH is on average 10% higher below the canopy than above. Similar patterns are found on growing season averages, with values of 57% at DA, 71% at NA and 81% at BE and an 8% drop between below- and above-canopy RH at BE. Daily RH is approximately 6% higher than diurnal RH at all three sites. The variability of RH at NA and DA is presented on Figure 4.

3.2. Triple Oxygen Isotopic Compositions of Precipitation, Groundwater, Soil Water, and Plant Water

At NA, the precipitation annual weighted average in $\delta'^{18}O$ is -4.2 ± 2.4 ‰ in 2018 and -5.3 ± 2.6 ‰ in 2019. ^{17}O-excess and d-excess are similar (22 ± 9 per meg in 2019–8 and 2019 for ^{17}O-excess; 11.1 ± 4.1 ‰ in 2018 and 11.7 ± 3.0 ‰ in 2019 for d-excess). On the event-scale, precipitation ^{17}O-excess varies by 40–50 per meg, increasing from the beginning to the heart of the rainy season and decreasing thereafter (Figure 4). d-excess does not show such a clear evolution over time. At DA, the 2019 precipitation annual averages in $\delta'^{18}O$, d-excess and ^{17}O-excess are -5.2 ± 1.4 ‰, 10.1 ± 1.8 ‰ and 18 ± 6 per meg, respectively, that is, close to NA annual averages. Interestingly, during the rainy season at DA, the evolution of ^{17}O-excess is roughly superimposed on that of NA at the same time (Figure 4).

Groundwater and tapwater sampled in August 2019 at DA have $\delta'^{18}O$ close to that of DA 2019 annual weighted average precipitation (0.7 ‰ difference). d-excess and ^{17}O-excess are respectively slightly lower (3.1 ‰) and higher (11 per meg). At NA, groundwater sampled regularly in 2018 and 2019 has a $\delta'^{18}O$ average 1.3 ‰ higher than the 2018–2019 NA annual weighted average precipitation. d-excess and ^{17}O-excess of groundwater are close to the annual weighted average precipitation (1.2 ‰ and 7 per meg difference, respectively).

The water from 10 soil cores taken at BE, NA and DA at the beginning and heart of the rainy season, was successfully extracted by centrifugation. In contrast, in soil cores taken during the dry season, centrifugation failed to extract any water. At the beginning of the rainy season, the water content ranges from 1% to 7% in DA and NA soils samples and from 8% to 10% in BE soils (Figure 5). At the heart of the rainy season, the water content ranges from 7% to 12% in NA soils, from 11% to 22% in BE soils. As a reminder, the DA soil was not cored at the heart of the rainy season. There is no correlation between the amount of water content and the proportion of extracted water. Variations of $\delta'^{18}O$ and d-excess with depth (standard deviation on the average, per soil profil) are respectively lower than 1‰ and 5‰. The ^{17}O-excess presents large uncertainties (up to 28 per meg) because it could only be measured once. This large uncertainty prevents further interpretation of the ^{17}O-excess variation with depth.

The isotopic composition of extracted soil water can be compared to that of precipitation preceding the samplings (Figure 5). At NA, the differences are smaller at the heart of the rainy season (September 2018), when RH is maximum. At this time the $\delta'^{18}O$ of soil water exceeds by less than 1‰ that of precipitation at NA. The ^{17}O-excess of soil water is generally lower than that of precipitation by less than 15 per meg, excepted in the top horizon where the difference can reach 25 per meg. The d-excess is close but higher than that of precipitation. At the beginning of the rainy season, at NA and DA, the $\delta'^{18}O$ of soil water exceeds significantly that of precipitation, by up to 8 ‰. The ^{17}O-excess and d-excess are always lower than those of precipitation. The difference can reach 46 per meg for ^{17}O-excess in DA soil and 24‰ for d-excess in NA soil.

In the ^{17}O-excess versus $\delta'^{18}O$ space, precipitation, groundwater and soil water show a limited range of ^{17}O-excess compared to plant water (Figure 6). Stem water have low $\delta'^{18}O$ and high ^{17}O-excess, close to the isotopic composition of soil water, groundwater and precipitation. Grass leaf water reaches −110 per meg, at the beginning of the rainy season at NA. Tree leaf water reaches −252 per meg at BE (*Isoberlinia doka*) and −271 per meg at NA (*Parkia Biglobosa*), during the dry season. The slope of the correlation lines linking stem and leaf water isotopic compositions in the triple oxygen isotopic system, defined as $\lambda_{\text{leaf water-stem water}}$, is 0.518 ± 0.001.

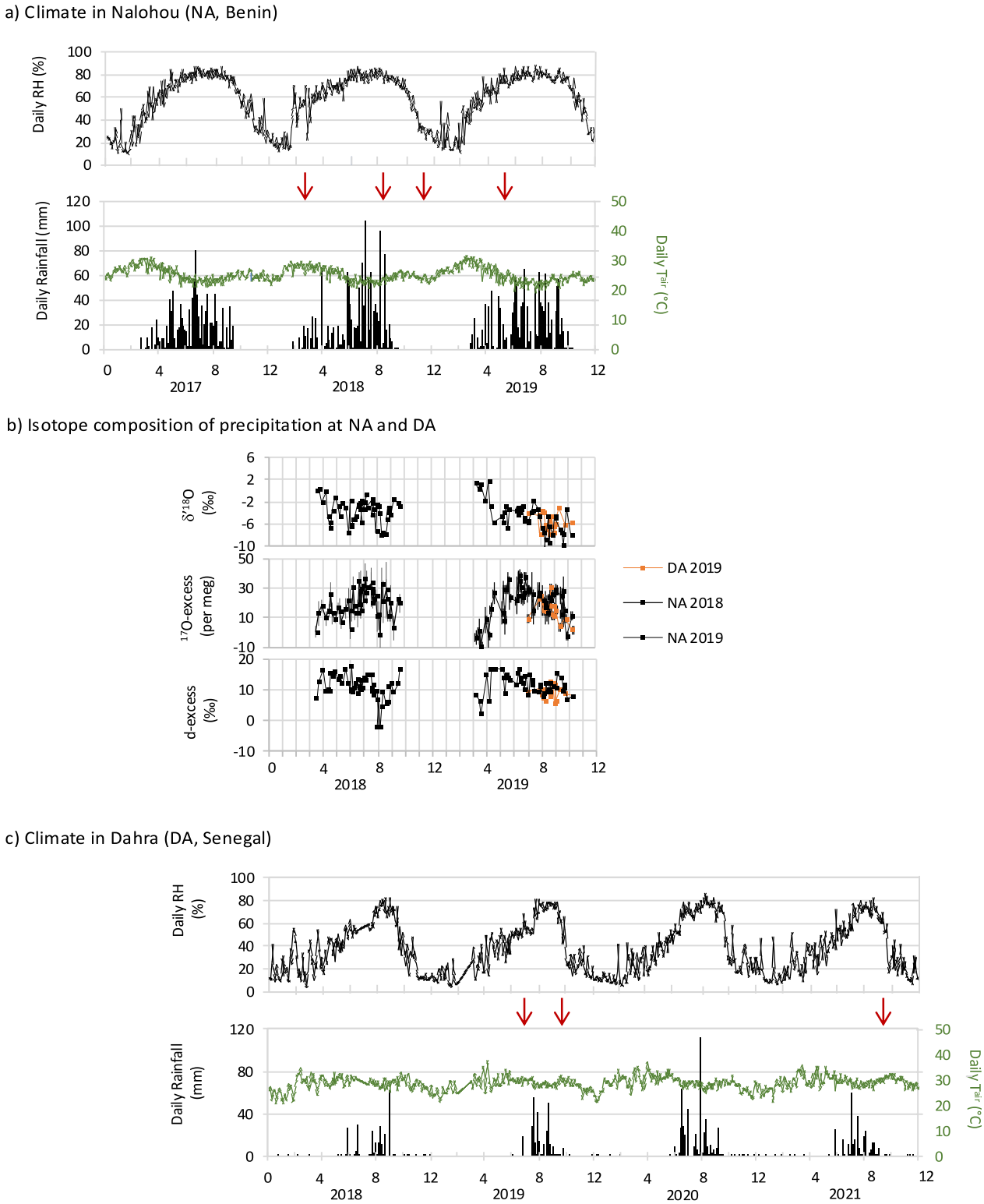

Figure 4. Daily precipitation, air temperature (T_{air}) and relative humidity (RH) variations preceding and during sample collections at the AMMA-CATCH sites of (a) Nalohou (NA) and (c) Dahra (DA). Arrows indicate the soil and plant sampling campaigns. (b) $\delta'^{18}O$, ^{17}O-excess and d-excess of precipitation at NA and DA. Error bars are not shown when they are smaller than the symbol. Raw data are available in Alexandre (2025).

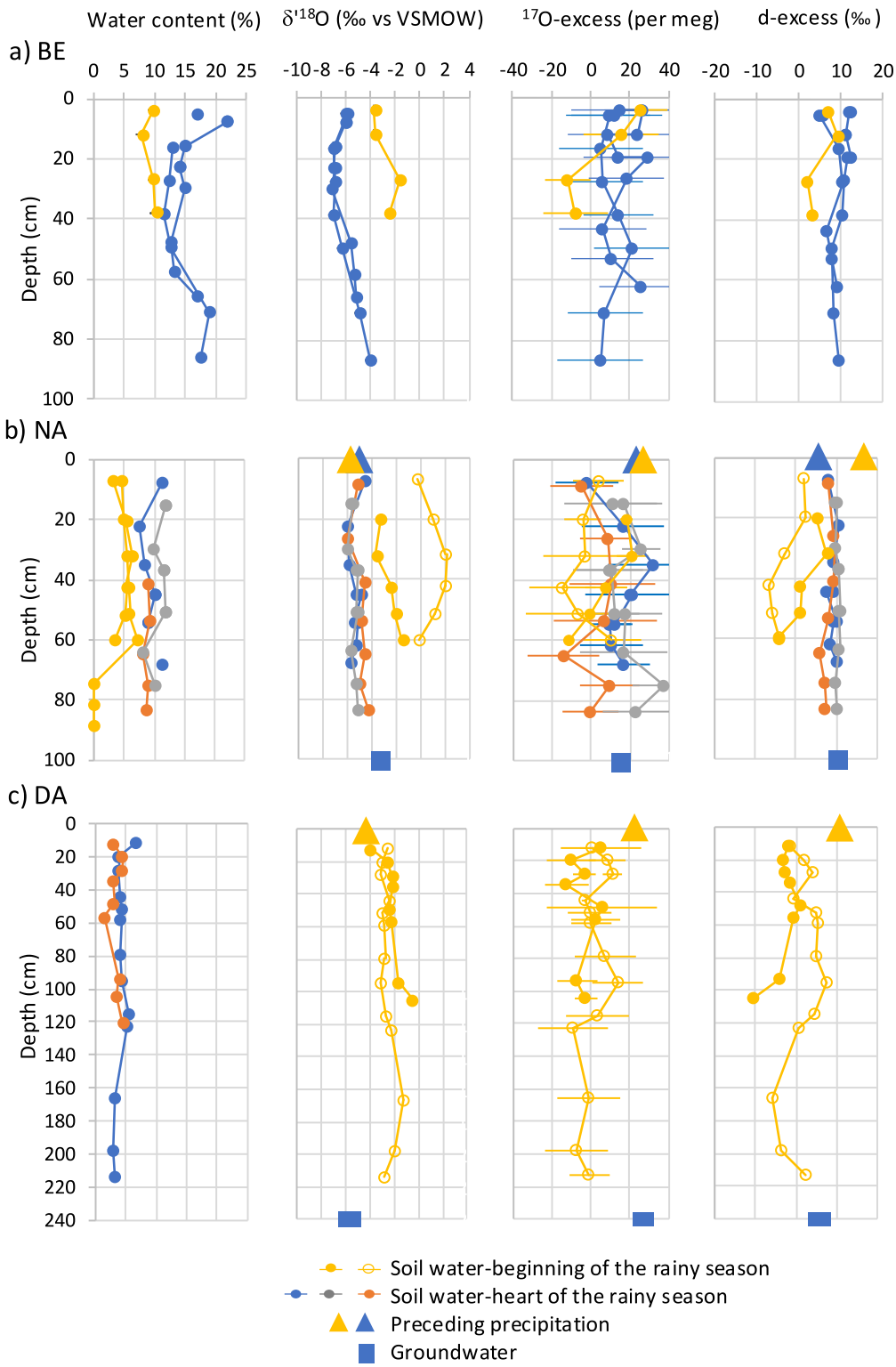

Figure 5. Soil water content, $\delta'^{18}O$, ^{17}O-excess and d-excess of centrifuged water versus depth for the 10 soil cores sampled from (a) Belefoungou (BE), (b) Nalohou (NA) and (c) Dahra (DA) at the beginning of the rainy season and at the heart of the rainy season. Isotopic compositions of the main precipitation event preceding the corings and of groundwater averages at NA and DA are also shown for comparison. When not indicated, error bars are included in the symbol size. Raw data are available in Alexandre (2025).

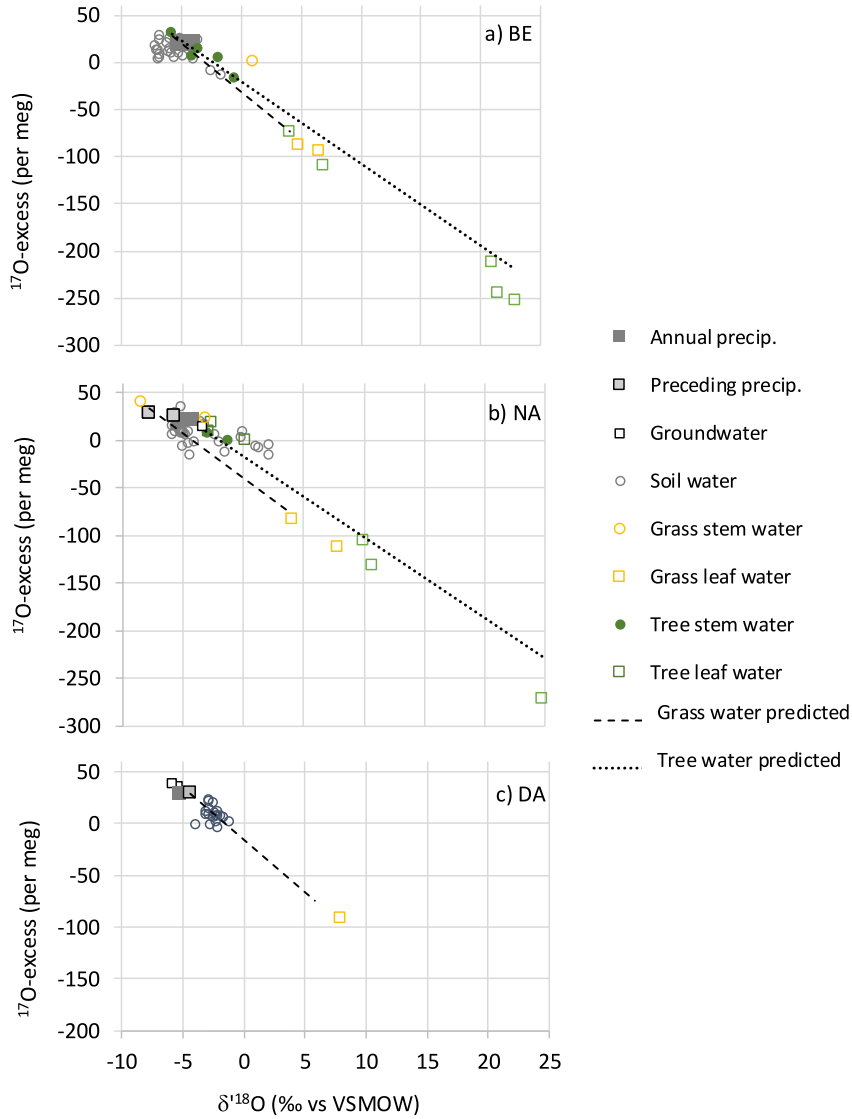

Figure 6. ^{17}O-excess versus δ′^{18}O measured for weighted average annual precipitation, groundwater, soil water, and plant water at (a) Belefoungou (BE; 2018–2019), (b) Nalohou (NA; 2018–2019), and (c) Dahra (DA; 2019). The lines connecting the predicted isotopic compositions for grass leaf waters and tree leaf waters during the rainy and dry seasons are shown. Raw data are available in Alexandre (2025).

3.3. Phytolith Concentration and Triple Oxygen Isotopic Composition

Phytolith concentration ranges from 0.2% to ca. 8% of dry weight (d.w.) in grasses. Leaves and sheaths contain generally one and a half to seven times more phytoliths than stems. Leaf phytoliths dominate the aboveground phytolith productions, ranging from 70% to 97% of the tussocks collected at BE and NA (Table 2). Senescent and growing grass samples show similar phytolith contents, which means that silicification stops when senescence starts.

When ^{17}O-excess versus δ′^{18}O of grass phytoliths are plotted, they show a strong negative correlation (Figure 7). In the δ′^{17}O versus δ′^{18}O space, the slope of the line linking leaf and stem phytoliths, that is, $\lambda_{\text{leaf phytolith-stem phytolith}}$ is 0.517 ± 0.001, that is, close to $\lambda_{\text{leaf water-stem water}}$ average measured and presented in Section 3.2 (0.518 ± 0.001).

To estimate the apparent fractionation between phytoliths and water, we calculated the fractionation observed between the isotopic compositions of stem phytoliths and precipitation of the growth period ($\Delta'^{18}O_{\text{phyto-P}}$ and Δ^{17}O-excess$_{\text{phyto-P}}$) (10 pairs). Growth period precipitation average was weighted by precipitation amount in

Table 2
Biomass, Phytolith Concentration, $\delta'^{18}O$, and ^{17}O-excess of Phytoliths From Stems, Sheaths and Leaves of Senescent (Sen) and Growing Andropogon Gayanus (AndroG), Imperata Cylindrica (Imp.C) and Hyparrhenia Involucrata (HypI) Collected at BE and NA

Grass species and sampling date	Biomass proportion (%)		Phytolith concentration (% biomass d.w.)		Phytolith proportion (%)		Phytolith measured				Phytolith calculate	
							$\delta'^{18}O$ ‰	^{17}O-excess per meg	$\delta'^{18}O$ ‰	17O-excess per meg	$\delta'^{18}O$ ‰	^{17}O-excess per meg
	Leaf + sheath	Stem	Leaf + sheath	Stem	Leaf + sheath	Stem	Leaf + sheath		stem		Bulk (stem, sheath and leaf)	
BE-200519 AndroG sen	0.7	0.3	1.3	0.8	78	22	30.05	−192	29.44	−165	35.59	−266
BE-030123 AndroG, Imp C growing	0.5	0.5	3.0	0.1	97	3	30.68	−211	30.78	−184	30.68	−210
NA-190519 AndroG sen	0.7	0.3	2.9	2.8	70	30	32.11	−228	30.62	−182	31.67	−214
NA-190519 HypI sen	0.3	0.7	7.5	0.9	78	22	30.77	−147	28.01	−171	30.15	−153
NA-030123 AndroG, HypI growing	0.6	0.4	2.8	0.4	91	9	36.05	−276	30.70	−158	35.59	−266

Note. The $\delta'^{18}O$ and ^{17}O-excess of a bulk sample of phytoliths is calculated. Raw data are available in Alexandre (2025).

addition to silicification rate (Equation 11). $\Delta'^{18}O_{\text{phyto-P}}$ and $\Delta^{17}O\text{-excess}_{\text{phyto-P}}$ are 32.42 ± 1.25 ‰ and −182 ± 23 per meg, respectively. The associated observed fractionation coefficient in the $\delta'^{17}O$ versus $\delta'^{18}O$ space, denoted $\lambda_{\text{phyto-P}}$, is 0.522 ± 0.0006. It is in the range of apparent fractionation coefficients obtained for the growth chamber calibrations and for a subsample of stem phytoliths from NA and BE previously published (Outrequin et al., 2021).

3.4. ^{17}O-Excess of Phytoliths Versus RH

The $^{17}O\text{-excess}_{\text{phyto}}$ of grass leaves shows a trend with daily and diurnal RH averages (weighted for growth and silicification rate) of the growth period (Figure 8). The majority of samples fall within the growth chamber calibration domain (Outrequin et al., 2021) when daily RH is considered (Figure 8a) but outside when diurnal RH is considered (Figure 8b). When RH values are not weighted according to phytolith production, samples are shifted to the left with respect to the calibration domain, due to the 5 ± 2% difference between weighted and unweighted RH averages, but remain mostly within the calibration range (not shown). Therefore, if the growth chamber $^{17}O\text{-excess}_{\text{phyto}}$ versus RH calibration is taken as a reference, weighted daily RH rather than weighted diurnal RH is recorded by $^{17}O\text{-excess}_{\text{phyto}}$ of grass leaves from BE, NA and DA.

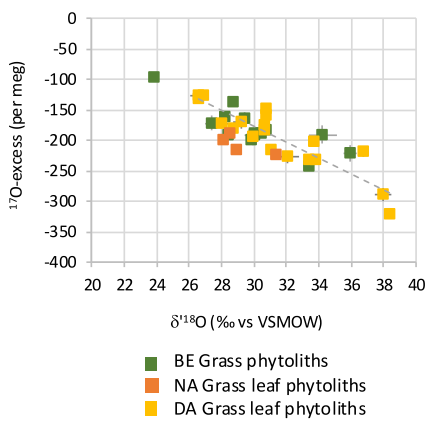

Figure 7. ^{17}O-excess versus $\delta'^{18}O$ of phytoliths from grasses sampled at BE, NA and DA. Raw data are available in Alexandre (2025).

4. Discussion

Here we provide modern data on the triple oxygen isotopic evolution from precipitation to groundwater, soil water and plant water. These data can serve as a basis for examining exchange processes between those compartments of the water cycle, with a particular focus on the role of vegetation. These data are also helpful to assess the robustness of $^{17}O\text{-excess}_{\text{phyto}}$ as an indicator of RH governing plant transpiration and leaf water evaporation.

4.1. Uniformity of ^{17}O-Excess in Precipitation and Groundwater

From event to event, the $\delta'^{18}O$, d-excess and ^{17}O-excess in precipitation are not correlated (Figure 4). This lack of correlation has been previously discussed in the light of theorethical models (Xia et al., 2023), as presented in Section 1. In non-polar regions, the main drivers of variations in ^{17}O-excess in precipitation are (a) evaporation from the oceans, (b) mixing of several sources of water vapor, including terrestrial moisture, and (c) evaporation from raindrops. Interpreting the triple oxygen isotopic composition of precipitation at the event scale is not the purpose of the present paper. More long-

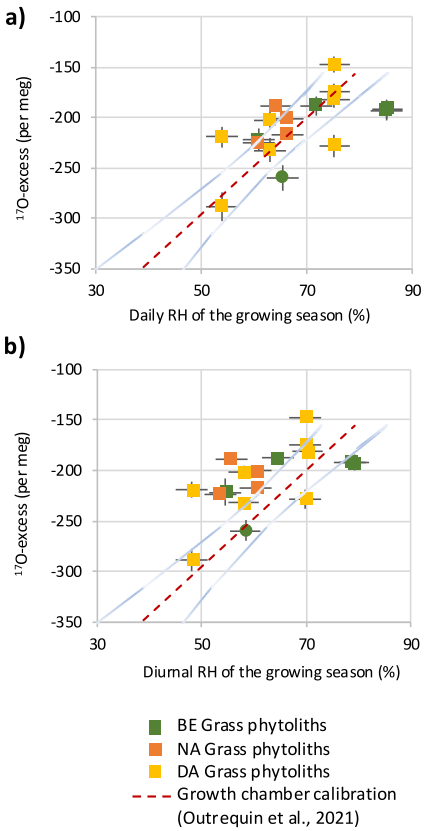

Figure 8. $^{17}O\text{-excess}_{phyto}$ of grass leaf from BE, NA and DA versus (a) daily RH and (b) diurnal RH of the growth season measured on site. The growth chamber calibration domain (Equation 10 with 95% confidence interval) is shown for comparison. RH data are weighted for grass growth and silicification rate. Error bars on $^{17}O\text{-excess}_{phyto}$ values represent the SD obtained for 2 to 4 replicates. Error bars on RH are set at ± 3% (1 SD). Raw data are available in Alexandre (2025).

term observations are needed to feed model-data approaches (Risi et al., 2013), assess the interactions over time between the drivers cited above, and simulate the short-term variability of $\delta'^{18}O$, d-excess and ^{17}O-excess in precipitation.

The annual weighted average ^{17}O-excess in precipitation is similar across years and study (20 ± 3 per meg). This is in agreement with the few annual or multi-year records published to date, that show small variations in the average annual ^{17}O-excess in precipitation (Aron et al., 2021; He et al., 2021; Kaseke et al., 2018; Liang et al., 2024). On the scale of sub-orbital cycles, we expect the variability of ^{17}O-excess in precipitation, due to changes in oceanic conditions or continental moisture recycling, to be small relative to the associated analytical uncertainty. This is a major advantage for climate reconstructions based on biogenic or authigenic minerals, as it limits the number of factors influencing the variability of their ^{17}O-excess.

The proximity of the triple oxygen isotopic composition of the groundwater to the annual average of precipitation at NA and DA (Figure 5) supports their multi-year recharge by current precipitation. This is in agreement with the results of hydrological studies already carried out at the NA site (Kotchoni et al., 2018; Séguis et al., 2011).

4.2. Evaporation and Mixing of Soil Water: Model-Data Comparison

A model-data approach can be used to interpret the isotopic composition of soil water at DA and NA, at the beginning of the rainy season, when there is sufficient water in the soil to be extracted and the diurnal RH is the lowest of the rainy season, favoring evaporation (Figure 9). Modeled curves showing the isotopic composition of evaporated water as a function of the fraction evaporated (also a function of time) are presented in the diagrams ^{17}O-excess versus $\delta'^{18}O$ and d-excess versus $\delta^{18}O$. When a mixing equation between unevaporated water and highly evaporated water is added to the model, distinct curves are generated in the ^{17}O-excess versus $\delta'^{18}O$ system.

The isotopic composition of the waters circulating in the coarse pores (extracted by centrifugation) of the soil cores lie at the beginning of the curves. The high uncertainties associated with these data make it impossible to distinguish whether the waters have had little time to evaporate, or whether they are composed of a mixture of evaporated and non-evaporated water. As for the water circulating in the coarse and fine pores (extracted by cryogenic distillation), they are clearly located on the mixing curves. This suggests that in fine pores, likely more abundant in the loamy soil at NA than in the sandy soil at DA, there is highly evaporated water diluted in non-evaporated water either percolating downward or upward by capillarity. Evaporated water accounts for around 10% of bulk water in the sandy soil at DA and 20% in the loamy soil at NA.

Besides evaporation and mixing processes, two other mechanisms can affect the isotopic composition of soil water: (a) adsorption of water on soil particles (Lin et al., 2018; Oerter et al., 2014), especially in dry soils or in clay soils with high cation exchange capacity, can counteract the effect of evaporation on non-adsorbed water. As adsorption involves hydrogen bonds, it should affect primarily the d-excess signal. However, the d-excess and ^{17}O-excess are positively correlated in soil water sampled at the beginning of the rainy season, arguing against the importance of this process; (b) soil dewatering by plants, by uptaking a water pool rather than another, can modify the isotopic composition of bulk water remaining in the soil. However at NA and DA, grasses dominate and are little developed at the beginning of the rainy season, which exclude dewatering as a process impacting significantly the isotopic composition of soil water at this time of the growth season.

This model-data approach supports that several waters of different age and circulation make up bulk soil water (Sprenger & Allen, 2020). Furthermore, the lateral heterogeneity of the waters making up the bulk soil water is illustrated by the $\delta'^{18}O$ difference of the two soil cores taken less than a meter apart at NA (Figure 9b).

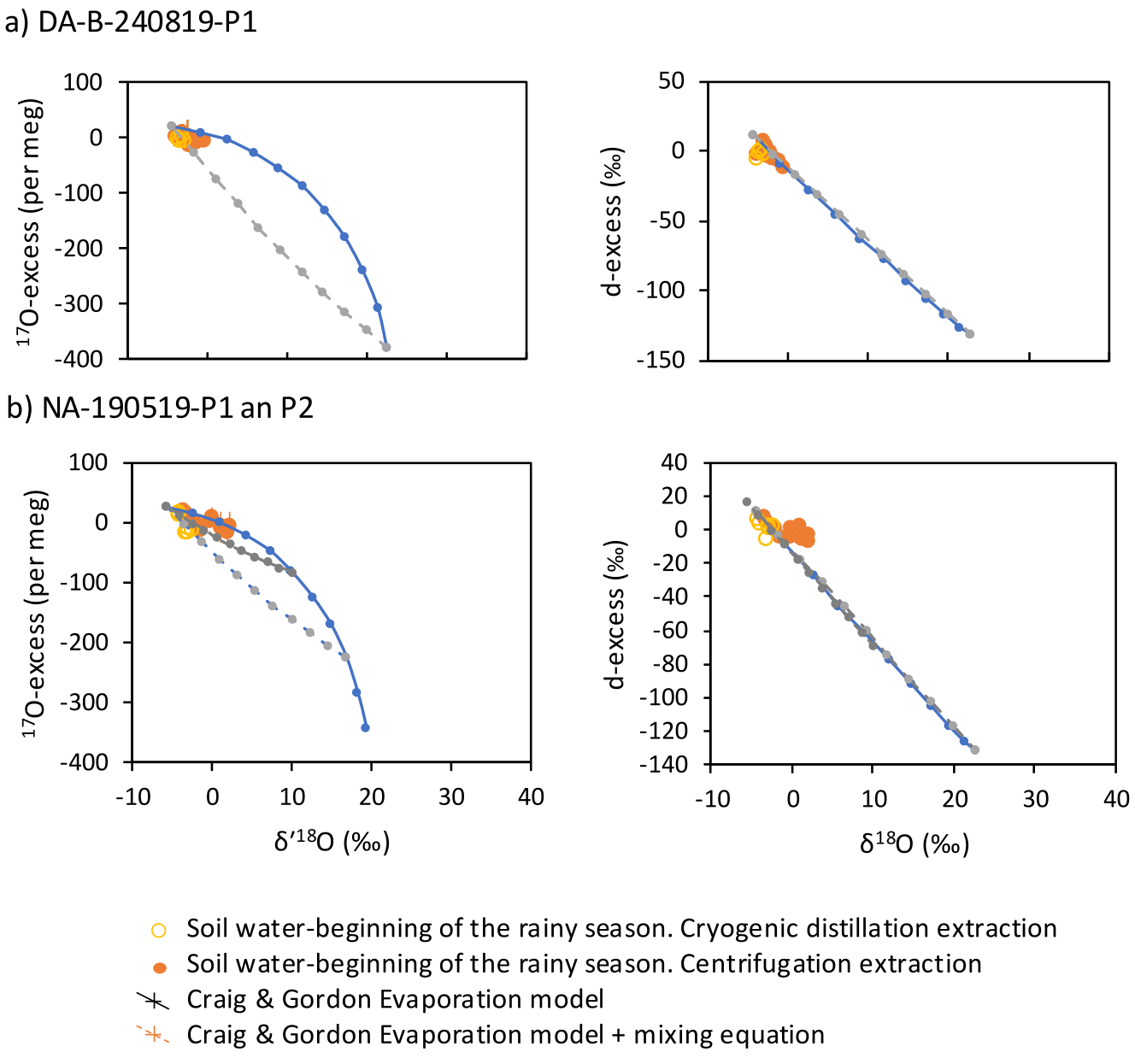

Figure 9. ^{17}O-excess versus δ'^{18}O and d-excess versus δ^{18}O of soil waters predicted using the Craig and Gordon evaporation model applied to an isolated volume of water, to which a mixing equation between evaporated and non-evaporated water pools was added (Voigt et al., 2021). Conditions are those of the beginning of the rainy season, observed on the day of soil coring (a) in Dahra (Senegal) (2019, August 24) and (b) in Nalohou (Benin) (2019, May 19). For the evaporation model, crosses indicate the proportion of residual water. For the evaporation + mixing equation model, crosses indicate the proportion of water evaporated. Isotopic measurements of soil water extracted by centrifugation and cryogenic distillation from Dahra sandy soil (core DA-B-240819-P1) and Nalohou silty soil (cores NA-190519-P1 and P2) are shown for comparison. Where not shown, error bars are included in the symbol size. Modeled and observed data are available in Alexandre (2025).

Unfortunately, due to the lack of isotopic soil water data for the dry season, we are unable to obtain a complete picture of evaporation and soil water circulation processes. Continuous in situ triple oxygen isotope monitoring of soil water could contribute to a better understanding of water circulation in soils.

4.3. Relationship Between Leaf Water and RH: Model-Data Comparison

The triple oxygen isotopic compositions of grass and tree leaf water predicted were compared to the observed values (Figure 6). Overall, observed δ'^{18}O and ^{17}O-excess between the leaf water and the initial water increases

when RH decreases, in agreement with the model, for grasses and trees. This confirms that evaporation drives the isotopic composition of the plants water, regardeless of the plant type.

For trees, the observed and modeled impact of evaporation on the $\delta'^{18}O$ and ^{17}O-excess of leaf water are in agreement. For grasses, it is underestimated (up to 78 per meg difference for ^{17}O-excess). This underestimation is too large to be explained by an underestimation of the isotopic composition of the initial water in the model, but can have other causes listed below. (a) Despite careful and rapid handling of the grass samples, evaporation can have occurred during the conditioning, which would have increased the measured $\delta'^{18}O$ and decreased the measured ^{17}O-excess. A systematic incorrect handling is however unlikely. (b) A near-zero difference of temperature between leaves and air used for calculating the ratio of water vapor mole fractions in the atmosphere and at the leaf evaporation site in the model, would also bring the predicted and observed values closer. During the samplings at the three sites, punctual measurements of T_{leaf} was done on the adaxial side of some grass leaves randomly selected, using an Optris CT IR thermometer (Optris GmbH, Berlin, Germany). These measurements (not shown) showed that although highly variable from a grass leaf to another, in relation to sun exposure, T_{leaf} was always equal to or lower than T_{air}, which makes this assumption possible. (c) At the contact of the grass leaves, RH 10%–15% lower than RH measured at 2 m height, used in the model, could explain the discrepancy. However, there are no measurements to assess this hypothesis. (d) A near-zero contribution of unevaporated vein water to the bulk leaf water considered in the model would bring the predicted values closer to the observed ones. This can be the case when grasses are sampled in the early stage of growth. Likely, a combination of the above biases is responsible of the discrepancies between observed and predicted values obtained for the grasses.

4.4. Triple Oxygen Isotopic Composition of Plant Water: A Tool for Tracing Absorbed Water

In the ^{17}O-excess versus $\delta'^{18}O$ space, although the mixture between evaporated and non-evaporated water is represented by a curve (Figure 1c), if a straight line is passed between a highly evaporated mixture and a poorly evaporated mixture, this line points close to the isotopic composition of the non-evaporated water. By analogy, if we pass a straight line between the isotopic compositions of leaf water and the isotopic compositions of stem water collected at NA, we should be able to point to the isotopic composition of the initial water pumped by the plants. To test this, we separated the data into Group 1 gathering stem and leaf water from grasses and trees sampled during the rainy season at NA and BE, and Group 2 gathering stem and leaf water from trees sampled in the dry season at BE. The regression line associated with Group 1 has a slope of 10 per meg/‰ (equivalent to 0.518 in the $\delta'^{17}O$ vs. $\delta'^{18}O$ space) (Figure 10a). The regression line associated with Group 2 is parallel to but offset from that of Group 1. Whatever the sampling season, leaf water from *Parkia Biglobosa*, the only tree sampled at NA, has an isotopic signature close to Group 2 and is thus also considered in Group 2. To check that the initial waters identified were discriminable, a statistical approach was followed: (a) in order to account for analytical uncertainties, pairs of $\delta'^{18}O$ and ^{17}O-excess values of stem and leaf water are generated by adding to the measured values an error drawn from a normal distribution whose mean is equal to 0 and standard deviation is equal to the analytical uncertainty on $\delta'^{18}O$ and ^{17}O-excess (0. 1‰ and 6 per meg, respectively, see Section 2); (b) for each group, the linear regression equation $^{17}O\text{-excess} = f(\delta'^{18}O)$ (Figure 10b) is calculated using the perturbed values; (c) from this equation, the $\delta'^{18}O$ value of the initial water is calculated assuming a ^{17}O-excess of 20 per meg which is the average value of the water table and weighted precipitation at NA; (d) steps 1 to 3 are repeated 1,000 times to generate, for each group, a sample of $\delta'^{18}O$ values of the initial water (Figures 10c); and (e) the statistical difference between these two $\delta'^{18}O$ values of the initial water samples is verified using a two-sample *t*-test and a non-parametric two-sample Wilcoxon rank sum test. The estimated $\delta'^{18}O$ of the initial water is -5.07 ± 0.23 ‰ for Group 1, that is, close to the $\delta'^{18}O$ weighted average of precipitation preceding the samplings (-6.43 ± 1.48 ‰). For Group 2, it is -3.69 ± 0.27 ‰, that is, close to the NA water table average of -3.38 ± 0.28 ‰. $\delta'^{18}O$ values of the initial waters are statistically different (p-value $<2.10e^{-16}$).

This demonstrates that the triple oxygen isotopic composition of plant leaf and stem water can be used to indicate the $\delta'^{18}O$ of water absorbed by plant roots, provided sufficient data are available. During the dry season, assuming that the water table at BE (not measured) has the same isotopic composition as the NA water table, the trees in the BE dry forest extract water from this water table. During the rainy season, BE and NA grasses and BE trees pump the soil water directly fed by precipitation preceding sampling. *Parkia biglobosa* at NA feeds on water table whatever is the season.

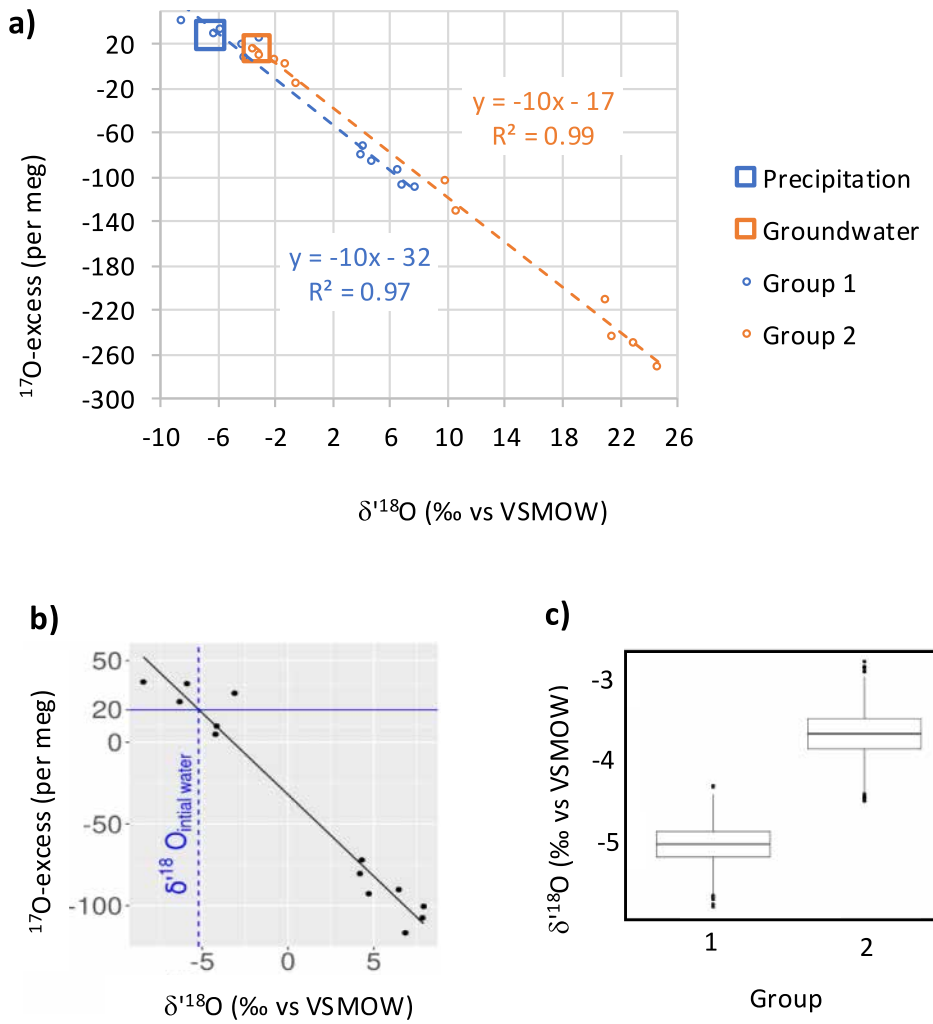

Figure 10. (a) ^{17}O-excess versus δ'^{18}O of stem and leaf waters from BE and NA, NA precipitation preceding the samplings average and NA water Tables 2018–2019 average. The regression lines linking stem and leaf water for Group 1 (NA and BE grasses and BE trees sampled at the heart of the rainy season) and Group 2 (BE trees sampled at the beginning of the rainy season and NA Parkia Biglobosa) point respectively to precipitation and water tables, whose symbols include error bars. (b) Graphic representation of the statistical estimation of the δ'^{18}O of initial water pumped by the roots. Black dots: measured ^{17}O-excess and δ'^{18}O of stem and leaf water perturbated with normally distributed random error (mean = 0; sd = analytical uncertainty); black line: regression line; dotted blue line: estimated δ'^{18}O of initial water for a ^{17}O-excess of 20 per meg (horizontal blue line); (c) Boxplot expressing the δ'^{18}O value of the initial water (with a ^{17}O-excess of 20 per meg) calculated for each of the two groups of plant water. Median (bold line), 25% and 75% quartiles, and extreme values (dots).

4.5. The Triple Oxygen Isotopic Fractionation Between Initial Water and Leaf Water Used for Estimating Biosphere Productivity

Knowledge of $\lambda_{\text{leaf water-initial water}}$ on a regional or global scale is necessary to quantify the contribution of the continental biosphere to the triple oxygen isotopic composition of O_2 and CO_2. The triple oxygen isotopic composition of atmospheric CO_2 and O_2 is used to assess the impact of vegetation to the global carbon cycle (Hofmann et al., 2017; Koren et al., 2019; Liang et al., 2024) or, when recorded in air bubbles of ices cores, to reconstruct past changes in gross primary production (Brandon et al., 2020; Luz et al., 1999; Yang et al., 2022). During photosynthesis oxygen is exchanged between water and CO_2 in the leaf and back-diffusion of the leaf CO_2 to the atmosphere occurs (Farquhar et al., 1993; Farquhar & Gan, 2003; Luz et al., 1999). Simultaneously, water is

split in the leaf to produce O_2 that contribute to atmospheric O_2. This contribution is balanced by O_2 plant consumption during respiration (e.g., Angert et al., 2003; Eisenstadt et al., 2010; Helman et al., 2005; Landais et al., 2007; Luz et al., 1999). The present study shows for BE and NA grasses and trees, the predicted $\lambda_{\text{leaf water-initial water}}$ is in the range 0.518 ± 0.001, in agreement with the observations. We can therefore use 0.518 ± 0.001 as $\lambda_{\text{leaf water-initial water}}$ for the tree and grass cover of the subhumid dry forest and savannas, as well as for the grass cover of the Sahelian savannas studied. This result is in agreement with the global value of 0.517 ± 0.001 previously published (Landais et al., 2006).

4.6. A Constant Apparent Triple Oxygen Isotopic Fractionation Between Plant Water and Phytoliths

The observed values of fractionation between pre-sampling precipitation and grass stem phytoliths ($\Delta'^{18}O_{\text{phyto-P}}$ and $\Delta^{17}O\text{-excess}_{\text{phyto-P}}$) are close to those predicted using the fractionation coefficient $^{18}\alpha_{\text{SiO2-H2O}}$ from Dodd and Sharp (2010) and a $\lambda_{\text{phyto-water}}$ of 0.522 obtained for previous calibrations in growth chamber (respectively, 30.64 ± 0.30 ‰ and −184 ± 2 per meg). As expected, T_{air} of the grass growth periods which varies by 3°C only, does not have a significant impact on $\Delta^{17}O\text{-excess}_{\text{phyto-P}}$ and $\lambda_{\text{phyto-H2O}}$ values. Taking the value of 0.524 calculated for equilibrium between water and silica (Cao & Liu, 2011; Sharp et al., 2016) would lead to a $\Delta^{17}O\text{-excess}_{\text{phyto-P}}$ of −123 ± 1 per meg, very far from the observed value. The apparent $\lambda_{\text{phyto-water}}$ of 0.522 can be explained by the heterogeneity of waters from which phytolith form over the course of leaf silicification. Previous measurement and modeling of the triple oxygen isotopic composition of phytoliths along a grass leaf shows that apparent $\lambda_{\text{phyto-water}}$ decreases from the base (0.523) to the apex (0.521) of the leaves, making 0.522 an average for the whole leaf, regardless of the length of the leaf (Alexandre et al., 2019). In the end, all the phytolith studies show that the apparent $\lambda_{\text{phyto-water}}$ of 0.522 ± 0.001 is obtained systematically for grass phytolith assemblages, regardless of the grass species (Alexandre et al., 2018, 2019; Guo et al., 2025; Outrequin et al., 2021; Voigt et al., 2023). This is an important point for using $^{17}O\text{-excess}_{\text{phyto}}$ as an indicator of RH driving plant water evaporation.

4.7. Which Accuracy for the Proxy of RH? Ajouter Apport Du Monitoring

If the calibration between ^{17}O-excess phyto and RH established under controlled growth chamber conditions is taken as a reference, the ^{17}O-excess phyto of grass leaves from BE, NA, and DA appears to record daily RH rather than diurnal RH (Figure 8). This contrasts with the isotopic compositions of grass phytoliths from Mediterranean and temperate sites, whose variations indicates that transpiration and hence silicification essentially occurs during the day (Guo et al., 2025; Voigt et al., 2023). This is however consistent with a recent synthesis examining 176 species worldwide that showed that, unlike Mediterranean and temperate species, tropical trees and grasses and tropical and xeric biomes have nighttime stomatal conductance representing 30%–50% of diurnal stomatal conductance (Resco de Dios et al., 2019; Siddiq & Cao, 2018).

Our study makes it possible to determine the RH recorded by grass leaf phytoliths in West African savanna and dry forest vegetation. However, for paleoclimate reconstruction purpose, bulk phytolith assemblages from sediments are used. In addition to grass leaf phytoliths, they can contain stem phytoliths and tree stem and leaf phytoliths. They may also be subject to taphonomic processes that can slightly modify the bulk isotopic composition and distort the RH reconstruction. Using the biomass, phytolith content and triple oxygen isotopic composition of stems, sheathes and leaves of 5 grass tussocks of *Andropogon gayanus, Imperata cylindrica*, and *Hyparrhenia involucrata* collected at BE and NA, the reconstructed RH distortion coming from stem phytolith contribution in the bulk phytolith assemblage can be estimated (Table 2). It is lower than 15 per meg on $^{17}O\text{-excess}_{\text{phyto}}$, which corresponds to a 3% overestimation of RH. This slight overestimation must be kept in mind when the $^{17}O\text{-excess}_{\text{phyto}}$ of bulk phytolith assemblages from soils and sediments is interpreted in terms of RH using (Equation 10).

5. Conclusion

The results presented here provide information on the amplitude of variations in the triple oxygen isotopic composition of water at the soil-plant-atmosphere interface in the West African savanna and dry forest contexts. The followed approach which compares data and model, makes up for the low number of data and help to characterize exchanges in the water cycle:

- Precipitation monitoring shows that the annual ^{17}O-excess stays around 20 per meg from one year to the next and from one site to the other. The low variability of ^{17}O-excess in precipitation on an annual scale, is a strong argument for using ^{17}O-excess in biogenic minerals as a paleoenvironmental indicator.
- δ'^{18}O and ^{17}O-excess of soil water are controlled by evaporation and mixing and show a limited contribution of evaporated water at the beginning of the rainy season. No data are available for the dry season.
- The regression line linking the triple oxygen isotopic composition of leaf and stem water allows us to determine the origin of the water absorbed by the roots. During the rainy season, grasses and trees absorb soil water fed by precipitation, which circulates rapidly and has no time to evaporate. In contrast, semi-evergreen trees reach water coming from the water table during the dry season.
- The triple oxygen isotopic composition of plant water evolves with RH according to a trend predicted by the Craig and Gordon model. It reaches −110 per meg in grasses at the beginning of the rainy season and −271 per meg in semi-evergreen trees, during the dry season.

This climatic and isotopic monitoring additionally enables us to specify the climatic proxy that is the ^{17}O-excess of phytoliths:

- We confirm that the apparent $\lambda_{\text{phyto-water}}$ of 0.522 ± 0.001 is obtained systematically for grass phytolith assemblages, whatever the grass species, which is a prerequisite for using a unique equation to estimate RH from $^{17}\text{O-excess}_{\text{phyto}}$.
- The previous growth chamber calibration between $^{17}\text{O-excess}_{\text{phyto}}$ and RH (Equation 10) applies to grass leaf phytoliths from the semi-arid and sub-humid West African savanna and dry forest sites studied. In this eco-climatic context, the ^{17}O-excess of grass leaf phytoliths records the daily RH during the growth season. The contribution of grass stem phytoliths to bulk phytolith assemblages should not bias RH estimates toward high values by more than 3%.

These insights contribute to better understand how to use the triple oxygen isotopic composition of water and phytoliths to constrain the present and past water cycles. Several avenues of research can now be explored:

- The event-to-event variability of precipitation in triple oxygen isotopic composition may point to physical processes that deserve to be investigated for a better understanding of the origin of air masses feeding precipitation, continental recycling and convective activity in the West African monsoon system.
- Unlike the d-excess versus δ^{18}O system, the ^{17}O-excess versus δ'^{18}O system is particularly adapted to distinguish water evaporation and mixing. Therefore, the triple oxygen isotopic analysis of soil water can be further developed to better constrain the complex hydrological functioning of soils and set up adapted hydro-isotopic models.
- The triple oxygen isotopic composition of stem and leaf water can be used to determine the water absorbed by roots in different contexts where the isotopic compositions of the potential water sources are a priori different. This is not the case for d-excess that may be biased in plants by surface tension effects or hydrogen exchange with organic compounds (Barbeta et al., 2018).
- Our results confirm the small variability in the ^{17}O-excess of precipitation compared to the very large magnitude of change in the ^{17}O-excess of phytoliths in response to changes in RH, demonstrating the relevance of ^{17}O-excess for climate reconstructions. To make the RH proxy even more accurate, the RH recorded by tree phytoliths from dry and humid forests now needs to be examined in more details. This will bring us closer to a single indicator for simultaneously reconstructing past vegetation and climate changes in West Africa.

Inclusion in Global Research

This study was carried out within the framework of long-term collaboration agreements between IRD and ISRA-CRZ in Senegal, and IRD and DG-Eau (Direction Générale de l'Eau) in Benin. All AMMA-CATCH sampling sites were equipped with the agreement of local authorities and communities. Our warmest thanks go to Mr. Dia Werima of Nalohou (Benin), who collected rain samples for isotopic analysis.

Conflict of Interest

The authors declare no conflicts of interest relevant to this study.

Data Availability Statement

All isotopic and climate data sets used in this study are available in Alexandre (2025). Raw climate data sets for BE and NA sites (Benin) are also available in AMMA-CATCH (1999, 2002, 2005).

Acknowledgments
This study was conducted in the framework of the HUMI-17 and PAST-17 projects supported by the ANR (ANR-17-CE01-0002-01 and ANR-22-CE01-0027-01), CNRS FR3098 ECCOREV, LABEX OT-Med, and OSU-Pytheas (France). JA and CV have benefited from a Marie Sklodowska-Curie Grant from the European Union (n° 101026211 for JA and 101063961 for CV). TT is affiliated with BECC, and acknowledge funds from FORMAS (Dnr 2021-00644; 2023-02436), the Swedish Space Agency (SNSA Dnr, 2021-00144; 2021-00111), Fysiografen, Carl Tryggers stiftelse, and the European Union under the Development Smart Innovation through Research in Agriculture (DeSIRA) Initiative (FOOD/2019/410-169). We thank C. Delon who provided the 2014 and 2017 evaporation and transpiration STEP simulations for DA. The observations used for Nalohou and Belefoungou sites were collected and processed by the AMMA-CATCH observatory (Galle et al., 2018). They are publicly available on the AMMA-CATCH database (http://dx.doi.org/10.17178/AMMA-CATCH.all). We thank Dr Cohard, Dr Mamadou, Dr Panthou for sharing these data sets, and all the technical staff involved in data collection and processing. We sincerely thank the reviewers for their thorough work, which greatly improved this study.

References

Agbohessou, Y., Delon, C., Mougin, E., Grippa, M., Tagesson, T., Diedhiou, M., et al. (2023). To what extent are greenhouse-gas emissions offset by trees in a Sahelian silvopastoral system? *Agricultural and Forest Meteorology*, *343*, 109780. https://doi.org/10.1016/j.agrformet.2023.109780

Alexandre, A., Basile-Doelsch, I., Sonzogni, C., Sylvestre, F., Parron, C., Meunier, J.-D., & Colin, F. (2006). Oxygen isotope analyses of fine silica grains using laser-extraction technique: Comparison with oxygen isotope data obtained from ion microprobe analyses and application to quartzite and silcrete cement investigation. *Geochimica et Cosmochimica Acta*, *70*(11), 2827–2835. https://doi.org/10.1016/j.gca.2006.03.003

Alexandre, A., Landais, A., Vallet-Coulomb, C., Piel, C., Devidal, S., Pauchet, S., et al. (2018). The triple oxygen isotope composition of phytoliths as a proxy of continental atmospheric humidity: Insights from climate chamber and climate transect calibrations. *Biogeosciences*, *15*(10), 3223–3241. https://doi.org/10.5194/bg-15-3223-2018

Alexandre, A. (2025). Climate and triple oxygen isotope of precipitation, groundwater, soil water, plant water, and phytolith data from West Africa (Benin and Senegal) [dataset bundled publication]. *PANGAEA*. https://doi.org/10.1594/PANGAEA.984133.

Alexandre, A., Webb, E., Landais, A., Piel, C., Devidal, S., Sonzogni, C., et al. (2019). Effects of leaf length and development stage on the triple oxygen isotope signature of grass leaf water and phytoliths: Insights for a proxy of continental atmospheric humidity. *Biogeosciences*, *16*(23), 4613–4625. https://doi.org/10.5194/bg-16-4613-2019

AMMA-CATCH. (1999). Precipitation dataset (5 minutes rainfall), over the Donga watershed (600 km2) [Dataset]. *Benin. IRD, CNRS-INSU, OSUG, OMP, OREME*. https://doi.org/10.17178/AMMA-CATCH.CL.Rain_Od

AMMA-CATCH. (2002). Meteorological dataset (including radiative budget), within the Donga watershed (600 km2) [Dataset]. *Benin. IRD, CNRS-INSU, OSUG, OMP, OREME*. https://doi.org/10.17178/AMMA-CATCH.AL.Met_Od

AMMA-CATCH. (2005). Surface flux dataset (including meteorological data, radiative budget, surface energy, water vapor and carbon fluxes), within the Donga watershed (600 km^2) [Dataset]. *Benin. IRD, CNRS-INSU, OSUG, OMP, OREME*. https://doi.org/10.17178/AMMA-CATCH.AE.H2OFlux_Odc

AMMA-CATCH. (2024). African monsoon multidisciplinary analysis: Coupling the tropical atmosphere and the hydrological cycle. Retrieved from https://www.amma-catch.org

Angert, A., Rachmilevitch, S., Barkan, E., & Luz, B. (2003). Effects of photorespiration, the cytochrome pathway, and the alternative pathway on the triple isotopic composition of atmospheric O_2. *Global Biogeochemical Cycles*, *17*(1), 1030. https://doi.org/10.1029/2002GB001933

Aron, P. G., Levin, N. E., Beverly, E. J., Huth, T. E., Passey, B. H., Pelletier, E. M., et al. (2020). Triple oxygen isotopes in the water cycle. *Chemical Geology*, *565*, 120026. https://doi.org/10.1016/j.chemgeo.2020.120026

Aron, P. G., Poulsen, C. J., Fiorella, R. P., Levin, N. E., Acosta, R. P., Yanites, B. J., & Cassel, E. J. (2021). Variability and controls on $\delta^{18}O$, d-excess, and $\Delta'^{17}O$ in Southern Peruvian precipitation. *Journal of Geophysical Research: Atmospheres*, *126*(23), e2020JD034009. https://doi.org/10.1029/2020JD034009

Awessou, K. G. B., Peugeot, C., Rocheteau, A., Seguis, L., Do, F. C., Galle, S., et al. (2017). Differences in transpiration between a forest and an agroforestry tree species in the Sudanian belt. *Agroforestry Systems*, *91*(3), 403–413. https://doi.org/10.1007/s10457-016-9937-8

Barbeta, A., Gimeno, T. E., Clavé, L., Fréjaville, B., Jones, S. P., Delvigne, C., et al. (2020). An explanation for the isotopic offset between soil and stem water in a temperate tree species. *New Phytologist*, *227*(3), 766–779. https://doi.org/10.1111/nph.16564

Barbeta, A., Ogée, J., & Peñuelas, J. (2018). Stable-Isotope techniques to investigate sources of plant water. In A. Sánchez-Moreiras & M. Reigosa (Eds.), *Advances in plant ecophysiology techniques*. Springer. https://doi.org/10.1007/978-3-319-93233-0_26

Barkan, E., & Luz, B. (2005). High precision measurements of $^{17}O/^{16}O$ and $^{18}O/^{16}O$ ratios in H_2O. *Rapid Communications in Mass Spectrometry*, *19*(24), 3737–3742. https://doi.org/10.1002/rcm.2250

Barkan, E., & Luz, B. (2007). Diffusivity fractionations of $H_2(^{16})O/H_2(^{17})O$ and $H_2(^{16})O/H_2(^{18})O$ in air and their implications for isotope hydrology. *Rapid Communications in Mass Spectrometry: Rapid Communications in Mass Spectrometry*, *21*(18), 2999–3005. https://doi.org/10.1002/rcm.3180

Beverly, E. J., Levin, N. E., Passey, B. H., Aron, P. G., Yarian, D. A., Page, M., & Pelletier, E. M. (2021). Triple oxygen and clumped isotopes in modern soil carbonate along an aridity gradient in the Serengeti, Tanzania. *Earth and Planetary Science Letters*, *567*, 116952. https://doi.org/10.1016/j.epsl.2021.116952

Brandon, M., Landais, A., Duchamp-Alphonse, S., Favre, V., Schmitz, L., Abrial, H., et al. (2020). Exceptionally high biosphere productivity at the beginning of Marine isotopic Stage 11. *Nature Communications*, *11*(1), 2112. https://doi.org/10.1038/s41467-020-15739-2

Cao, X., & Liu, Y. (2011). Equilibrium mass-dependent fractionation relationships for triple oxygen isotopes. *Geochimica et Cosmochimica Acta*, *75*(23), 7435–7445. https://doi.org/10.1016/j.gca.2011.09.048

Cernusak, L. A., Barbour, M. M., Arndt, S. K., Cheesman, A. W., English, N. B., Feild, T. S., et al. (2016). Stable isotopes in leaf water of terrestrial plants. *Plant, Cell and Environment*, *39*(5), 1087–1102. https://doi.org/10.1111/pce.12703

Corbineau, R., Reyerson, P. E., Alexandre, A., & Santos, G. M. (2013). Towards producing pure phytolith concentrates from plants that are suitable for carbon isotopic analysis. *Review of Palaeobotany and Palynology*, *197*, 179–185. https://doi.org/10.1016/j.revpalbo.2013.06.001

Craig, H., & Gordon, L. I. (1965). Deuterium and oxygen 18 variations in the Ocean and the marine atmosphere. *Consiglio nazionale delle richerche, Laboratorio de geologia nucleare*.

Crespin, J., Alexandre, A., Sylvestre, F., Sonzogni, C., Paillès, C., & Garreta, V. (2008). IR laser extraction technique applied to oxygen isotope analysis of small biogenic silica samples. *Analytical Chemistry*, *80*(7), 2372–2378. https://doi.org/10.1021/ac071475c

Di Bonito, M., Breward, N., Crout, N., Smith, B., & Young, S. (2008). Overview of selected soil pore water extraction methods for the determination of potentially toxic elements in contaminated Soils Operational and technical aspects. In *Environmental geochemistry: Site characterization, data analysis and case histories* (pp. 213–249). https://doi.org/10.1016/B978-0-444-53159-9.00010-3

Dodd, J. P., & Sharp, Z. D. (2010). A laser fluorination method for oxygen isotope analysis of biogenic silica and a new oxygen isotope calibration of modern diatoms in freshwater environments. *Geochimica et Cosmochimica Acta*, *74*(4), 1381–1390. https://doi.org/10.1016/j.gca.2009.11.023

Eisenstadt, D., Barkan, E., Luz, B., & Kaplan, A. (2010). Enrichment of oxygen heavy isotopes during photosynthesis in phytoplankton. *Photosynthesis Research*, *103*(2), 97–103. https://doi.org/10.1007/s11120-009-9518-z

Farquhar, G. D., & Gan, K. S. (2003). On the progressive enrichment of the oxygen isotopic composition of water along a leaf. *Plant, Cell and Environment*, *26*(6), 801–819. https://doi.org/10.1046/j.0016-8025.2001.00829.x-i1

Farquhar, G. D., Lloyd, J., Taylor, J. A., Flanagan, L. B., Syvertsen, J. P., Hubick, K. T., et al. (1993). Vegetation effects on the isotope composition of oxygen in atmospheric CO_2. *Nature*, *363*(6428), 439–443. https://doi.org/10.1038/363439a0

Fensholt, R., Sandholt, I., & Rasmussen, M. S. (2004). Evaluation of MODIS LAI, fAPAR and the relation between fAPAR and NDVI in a semi-arid environment using in situ measurements. *Remote Sensing of Environment*, *91*(3), 490–507. https://doi.org/10.1016/j.rse.2004.04.009

Fournier, A. (1991). *Phénologie, croissance et production végétales dans quelques savanes d'Afrique de l'Ouest: variation selon un gradient climatique*. Editions de l'ORSTOM.

Galle, S., Grippa, M., Peugeot, C., Moussa, I. B., Cappelaere, B., Demarty, J., et al. (2018). AMMA-CATCH, a critical Zone observatory in West Africa monitoring a Region in transition. *Vadose Zone Journal*, *17*(1), 180062-24. https://doi.org/10.2136/vzj2018.03.0062

Gázquez, F., Morellón, M., Bauska, T., Herwartz, D., Surma, J., Moreno, A., et al. (2018). Triple oxygen and hydrogen isotopes of gypsum hydration water for quantitative paleo-humidity reconstruction. *Earth and Planetary Science Letters*, *481*, 177–188. https://doi.org/10.1016/j.epsl.2017.10.020

Gonfiantini, R., Wassenaar, L. I., Araguas-Araguas, L., & Aggarwal, P. K. (2018). A unified Craig-Gordon isotope model of stable hydrogen and oxygen isotope fractionation during fresh or saltwater evaporation. *Geochimica et Cosmochimica Acta*, *235*, 224–236. https://doi.org/10.1016/j.gca.2018.05.020

Green, J. K., Zhang, Y., Luo, X., & Keenan, T. F. (2024). Systematic underestimation of canopy conductance sensitivity to drought by Earth System Models. *AGU Advances*, *5*(1), e2023AV001026. https://doi.org/10.1029/2023AV001026

Gröning, M., Lutz, H. O., Roller-Lutz, Z., Kralik, M., Gourcy, L., & Pöltenstein, L. (2012). A simple rain collector preventing water re-evaporation dedicated for $\delta^{18}O$ and $\delta^{2}H$ analysis of cumulative precipitation samples. *Journal of Hydrology*, *448–449*, 195–200. https://doi.org/10.1016/j.jhydrol.2012.04.041

Grossiord, C., Buckley, T. N., Cernusak, L. A., Novick, K. A., Poulter, B., Siegwolf, R. T. W., et al. (2020). Plant responses to rising vapor pressure deficit. *New Phytologist*, *226*(6), 1550–1566. https://doi.org/10.1111/nph.16485

Guo, M., Alexandre, A., Longstaffe, F. J., Peugeot, C., & Webb, E. (2025). ^{17}O-excess of grass leaf phytoliths across the North American prairies records late-growing season daytime relative humidity. *Chemical Geology*, *671*(2025), 122484. https://doi.org/10.1016/j.chemgeo.2024.122484

He, S., Jackisch, D., Samanta, D., Yi, P. K. Y., Liu, G., Wang, X., & Goodkin, N. F. (2021). Understanding tropical convection through triple oxygen isotopes of precipitation from the maritime continent. *Journal of Geophysical Research: Atmospheres*, *126*(4), e2020JD033418. https://doi.org/10.1029/2020JD033418

Hector, B., Cohard, J.-M., Séguis, L., Galle, S., & Peugeot, C. (2018). Hydrological functioning of western African inland valleys explored with a critical zone model. *Hydrology and Earth System Sciences*, *22*(11), 5867–5888. https://doi.org/10.5194/hess-22-5867-2018

Hector, B., Séguis, L., Hinderer, J., Cohard, J.-M., Wubda, M., Descloitres, M., et al. (2015). Water storage changes as a marker for base flow generation processes in a tropical humid basement catchment (Benin): Insights from hybrid gravimetry. *Water Resources Research*, *51*(10), 8331–8361. https://doi.org/10.1002/2014WR015773

Helman, Y., Barkan, E., Eisenstadt, D., Luz, B., & Kaplan, A. (2005). Fractionation of the three stable oxygen isotopes by oxygen-producing and oxygen-consuming reactions in photosynthetic organisms. *Plant Physiology*, *138*(4), 2292–2298. https://doi.org/10.1104/pp.105.063768

Herzog, A., Hector, B., Cohard, J.-M., Vouillamoz, J.-M., Lawson, F. M. A., Peugeot, C., & de Graaf, I. (2021). A parametric sensitivity analysis for prioritizing regolith knowledge needs for modeling water transfers in the West African critical zone. *Vadose Zone Journal*, *20*(6), e20163. https://doi.org/10.1002/vzj2.20163

Hirl, R. T., Schnyder, H., Ostler, U., Schäufele, R., Schleip, I., Vetter, S. H., et al. (2019). The ^{18}O ecohydrology of a grassland ecosystem – Predictions and observations. *Hydrology and Earth System Sciences*, *23*(6), 2581–2600. https://doi.org/10.5194/hess-23-2581-2019

Hofmann, M. E. G., Horvath, B., Schneider, L., Peters, W., Schützenmeister, K., & Pack, A. (2017). Atmospheric measurements of $\Delta^{17}O$ in CO_2 in Göttingen, Germany reveal a seasonal cycle driven by biospheric uptake. *Geochimica et Cosmochimica Acta*, *199*, 143–163. https://doi.org/10.1016/j.gca.2016.11.019

Hutchings, J. A., & Konecky, B. L. (2023). Optimization of a Picarro L2140-i cavity ring-down spectrometer for routine measurement of triple oxygen isotope ratios in meteoric waters. *Atmospheric Measurement Techniques*, *16*(6), 1663–1682. https://doi.org/10.5194/amt-16-1663-2023

Huth, T. E., Passey, B. H., Cole, J. E., Lachniet, M. S., McGee, D., Denniston, R. F., et al. (2022). A framework for triple oxygen isotopes in speleothem paleoclimatology. *Geochimica et Cosmochimica Acta*, *319*, 191–219. https://doi.org/10.1016/j.gca.2021.11.002

Kaseke, K. F., Wang, L., Wanke, H., Tian, C., Lanning, M., & Jiao, W. (2018). Precipitation origins and key drivers of precipitation isotope (^{18}O, ^{2}H, and ^{17}O) compositions over Windhoek. *Journal of Geophysical Research: Atmospheres*, *123*(14), 7311–7330. https://doi.org/10.1029/2018JD028470

Kelson, J. R., Huth, T. E., Passey, B. H., Levin, N. E., Petersen, S. V., Ballato, P., et al. (2023). Triple oxygen isotope compositions of globally distributed soil carbonates record widespread evaporation of soil waters. *Geochimica et Cosmochimica Acta*, *355*, 138–160. https://doi.org/10.1016/j.gca.2023.06.034

Koren, G., Schneider, L., van der Velde, I. R., van Schaik, E., Gromov, S. S., Adnew, G. A., et al. (2019). Global 3-D simulations of the triple oxygen isotope signature $\Delta^{17}O$ in atmospheric CO_2. *Journal of Geophysical Research: Atmospheres*, *124*(15), 8808–8836. https://doi.org/10.1029/2019JD030387

Kotchoni, D. O. V., Vouillamoz, J.-M., Lawson, F. M. A., Adjomayi, P., Boukari, M., & Taylor, R. G. (2018). Relationships between rainfall and groundwater recharge in seasonally humid Benin: A comparative analysis of long-term hydrographs in sedimentary and crystalline aquifers. *Hydrogeology Journal*, *27*(2), 447–457. https://doi.org/10.1007/s10040-018-1806-2

Landais, A., Barkan, E., Yakir, D., & Luz, B. (2006). The triple isotopic composition of oxygen in leaf water. *Geochimica et Cosmochimica Acta*, *70*(16), 4105–4115. https://doi.org/10.1016/j.gca.2006.06.1545

Landais, A., Lathiere, J., Barkan, E., & Luz, B. (2007). Reconsidering the change in global biosphere productivity between the Last Glacial Maximum and present day from the triple oxygen isotopic composition of air trapped in ice cores. *Global Biogeochemical Cycles*, *21*(1), GB1025. https://doi.org/10.1029/2006GB002739

Leroux, D. J., Pellarin, T., Vischel, T., Cohard, J.-M., Gascon, T., Gibon, F., et al. (2016). Assimilation of SMOS soil moisture into a distributed hydrological model and impacts on the water cycle variables over the Ouémé catchment in Benin. *Hydrology and Earth System Sciences*, *20*(7), 2827–2840. https://doi.org/10.5194/hess-20-2827-2016

Li, S., Levin, N. E., Soderberg, K., Dennis, K. J., & Caylor, K. K. (2017). Triple oxygen isotope composition of leaf waters in Mpala, central Kenya. *Earth and Planetary Science Letters*, *468*, 38–50. https://doi.org/10.1016/j.epsl.2017.02.015

Liang, Q.-S., Sha, L.-J., Li, J.-Y., Zhang, J., Wang, X.-J., Zhou, S.-L., et al. (2024). Seasonal variations and controls on triple oxygen and hydrogen isotopes in Precipitation: A Case Study from monitoring in Southwest China. *Journal of Geophysical Research: Atmospheres*, *129*(17), e2023JD040654. https://doi.org/10.1029/2023JD040654

Lin, Y., Horita, J., & Abe, O. (2018). Adsorption isotope effects of water on mesoporous silica and alumina with implications for the land-vegetation-atmosphere system. *Geochimica et Cosmochimica Acta*, *223*, 520–536. https://doi.org/10.1016/j.gca.2017.12.021

Liu, L., Gudmundsson, L., Hauser, M., Qin, D., Li, S., & Seneviratne, S. I. (2020). Soil moisture dominates dryness stress on ecosystem production globally. *Nature Communications*, *11*(1), 4892. https://doi.org/10.1038/s41467-020-18631-1

López, J. R., Schoppach, R., & Sadok, W. (2021). Harnessing nighttime transpiration dynamics for drought tolerance in grasses. *Plant Signaling and Behavior*, *16*(4), 1875646. https://doi.org/10.1080/15592324.2021.1875646

Luz, B., Barkan, E., Bender, M. L., Thiemens, M. H., & Boering, K. A. (1999). Triple-isotope composition of atmospheric oxygen as a tracer of biosphere productivity. *Nature*, *400*(6744), 547–550. https://doi.org/10.1038/22987

Luz, B., Barkan, E., Yam, R., & Shemesh, A. (2009). Fractionation of oxygen and hydrogen isotopes in evaporating water. *Geochimica et Cosmochimica Acta*, *73*(22), 6697–6703. https://doi.org/10.1016/j.gca.2009.08.008

Mamadou, O., Galle, S., Cohard, J.-M., Peugeot, C., Kounouhewa, B., Biron, R., et al. (2016). Dynamics of water vapor and energy exchanges above two contrasting Sudanian climate ecosystems in Northern Benin (West Africa). *Journal of Geophysical Research: Atmospheres*, *121*(19), 2016JD024749. https://doi.org/10.1002/2016JD024749

Mayaux, P., Bartholomé, E., Fritz, S., & Belward, A. (2004). Anew land-cover map of Africa for the year 2000. *Journal of Biogeography*, *31*(6), 861–877. https://doi.org/10.1111/j.1365-2699.2004.01073.x

Merlivat, L. (1978). Molecular diffusivities of $H_2{}^{16}O$, $HD^{16}O$, and $H_2{}^{18}O$ in gases. *The Journal of Chemical Physics*, *69*(6), 2864–2871. https://doi.org/10.1063/1.436884

Oerter, E., Finstad, K., Schaefer, J., Goldsmith, G. R., Dawson, T., & Amundson, R. (2014). Oxygen isotope fractionation effects in soil water via interaction with cations (Mg, Ca, K, Na) adsorbed to phyllosilicate clay minerals. *Journal of Hydrology*, *515*, 1–9. https://doi.org/10.1016/j.jhydrol.2014.04.029

Orlowski, N., Pratt, D. L., & McDonnell, J. J. (2016). Intercomparison of soil pore water extraction methods for stable isotope analysis. *Hydrological Processes*, *30*(19), 3434–3449. https://doi.org/10.1002/hyp.10870

Outrequin, C., Alexandre, A., Vallet-Coulomb, C., Piel, C., Devidal, S., Landais, A., et al. (2021). The triple oxygen isotope composition of phytoliths, a new proxy of atmospheric relative humidity: Controls of soil water isotope composition, temperature, CO_2 concentration and relative humidity. *Climate of the Past*, *17*(5), 1881–1902. https://doi.org/10.5194/cp-17-1881-2021

Passey, B. H., Hu, H., Ji, H., Montanari, S., Li, S., Henkes, G. A., & Levin, N. E. (2014). Triple oxygen isotopes in biogenic and sedimentary carbonates. *Geochimica et Cosmochimica Acta*, *141*, 1–25. https://doi.org/10.1016/j.gca.2014.06.006

Resco de Dios, V., Chowdhury, F. I., Granda, E., Yao, Y., & Tissue, D. T. (2019). Assessing the potential functions of nocturnal stomatal conductance in C3 and C4 plants. *New Phytologist*, *223*(4), 1696–1706. https://doi.org/10.1111/nph.15881

Risi, C., Landais, A., Winkler, R., & Vimeux, F. (2013). Can we determine what controls the spatio-temporal distribution of d-excess and 17O-excess in precipitation using the LMDZ general circulation model? *Climate of the Past*, *9*(5), 2173–2193. https://doi.org/10.5194/cp-9-2173-2013

Schoenemann, S. W., Schauer, A. J., & Steig, E. J. (2013). Measurement of SLAP2 and GISP $\delta^{17}O$ and proposed VSMOW-SLAP normalization for $\delta^{17}O$ and ^{17}O excess. *Rapid Communications in Mass Spectrometry*, *27*(5), 582–590. https://doi.org/10.1002/rcm.6486

Seghieri, J., Vescovo, A., Padel, K., Soubie, R., Arjounin, M., Boulain, N., et al. (2009). Relationships between climate, soil moisture and phenology of the woody cover in two sites located along the West African latitudinal gradient. *Journal of Hydrology*, *375*(1), 78–89. https://doi.org/10.1016/j.jhydrol.2009.01.023

Séguis, L., Kamagaté, B., Favreau, G., Descloitres, M., Seidel, J.-L., Galle, S., et al. (2011). Origins of streamflow in a crystalline basement catchment in a sub-humid Sudanian zone: The Donga basin (Benin, West Africa): Inter-annual variability of water budget. *Journal of Hydrology*, *402*(1), 1–13. https://doi.org/10.1016/j.jhydrol.2011.01.054

Sha, L., Wassenburg, J. A., Sha, L., Li, Y., Zhou, S., Liang, Q., et al. (2023). Variations in triple oxygen isotopic of speleothems from the Asian monsoon region reveal moisture sources over the past 300 years. *Communications Earth and Environment*, *4*(1), 1–10. https://doi.org/10.1038/s43247-023-01043-6

Sharp, Z. D., Gibbons, J. A., Maltsev, O., Atudorei, V., Pack, A., Sengupta, S., et al. (2016). A calibration of the triple oxygen isotopic fractionation in the SiO_2–H_2O system and applications to natural samples. *Geochimica et Cosmochimica Acta*, *186*, 105–119. https://doi.org/10.1016/j.gca.2016.04.047

Siddiq, Z., & Cao, K.-F. (2018). Nocturnal transpiration in 18 broadleaf timber species under a tropical seasonal climate. *Forest Ecology and Management*, *418*, 47–54. https://doi.org/10.1016/j.foreco.2017.12.043

Sprenger, M., & Allen, S. T. (2020). Commentary: What ecohydrologic separation is and where we can go with it. *Water Resources Research*, *56*(7), e2020WR027238. https://doi.org/10.1029/2020WR027238

Sprenger, M., Leistert, H., Gimbel, K., & Weiler, M. (2016). Illuminating hydrological processes at the soil-vegetation-atmosphere interface with water stable isotopes. *Reviews of Geophysics*, *54*(3), 674–704. https://doi.org/10.1002/2015RG000515

Suavet, C., Alexandre, A., Franchi, I. A., Gattacceca, J., Sonzogni, C., Greenwood, R. C., et al. (2010). Identification of the parent bodies of micrometeorites with high-precision oxygen isotope ratios. *Earth and Planetary Science Letters*, *293*(3–4), 313–320. https://doi.org/10.1016/j.epsl.2010.02.046

Surma, J., Assonov, S., & Staubwasser, M. (2021). Triple oxygen isotope systematics in the hydrologic cycle. *Reviews in Mineralogy and Geochemistry*, *86*(1), 401–428. https://doi.org/10.2138/rmg.2021.86.12

Tagesson, T., Fensholt, R., Guiro, I., Rasmussen, M. O., Huber, S., Mbow, C., et al. (2015). Ecosystem properties of semiarid savanna grassland in West Africa and its relationship with environmental variability. *Global Change Biology*, *21*(1), 250–264. https://doi.org/10.1111/gcb.12734

Terzer-Wassmuth, S., Araguás-Araguás, L. J., Wassenaar, L. I., & Stumpp, C. (2023). Global and local meteoric water lines for $\delta^{17}O/\delta^{18}O$ and the spatiotemporal distribution of $\Delta'^{17}O$ in Earth's precipitation. *Scientific Reports*, *13*(1), 19056. https://doi.org/10.1038/s41598-023-45920-8

Vallet-Coulomb, C., Couapel, M., & Sonzogni, C. (2021). Improving memory effect correction to achieve high-precision analysis of $\delta^{17}O$, $\delta^{18}O$, $\delta^{2}H$, ^{17}O-excess and d-excess in water using cavity ring-down laser spectroscopy. *Rapid Communications in Mass Spectrometry*, *35*(14), e9108. https://doi.org/10.1002/rcm.9108

Voigt, C., Alexandre, A., Reiter, I. M., Orts, J.-P., Vallet-Coulomb, C., Piel, C., et al. (2023). Examination of the parameters controlling the triple oxygen isotope composition of grass leaf water and phytoliths at a Mediterranean site: A model-data approach. *Biogeosciences*, *20*(11), 2161–2187. https://doi.org/10.5194/bg-20-2161-2023

Voigt, C., Herwartz, D., Dorador, C., & Staubwasser, M. (2021). Triple oxygen isotope systematics of evaporation and mixing processes in a dynamic desert lake system. *Hydrology and Earth System Sciences*, *25*(3), 1211–1228. https://doi.org/10.5194/hess-25-1211-2021

Webb, E. A., & Longstaffe, F. J. (2002). Climatic influences on the oxygen isotopic composition of biogenic silica in prairie grass. *Geochimica et Cosmochimica Acta*, *66*(11), 1891–1904. https://doi.org/10.1016/s0016-7037(02)00822-0

Wostbrock, J. A. G., & Sharp, Z. D. (2021). Triple oxygen isotopes in Silica–Water and carbonate–water systems. *Reviews in Mineralogy and Geochemistry*, *86*(1), 367–400. https://doi.org/10.2138/rmg.2021.86.11

Xia, Z., Surma, J., & Winnick, M. J. (2023). The response and sensitivity of deuterium and ^{17}O excess parameters in precipitation to hydroclimate processes. *Earth-Science Reviews*, *242*, 104432. https://doi.org/10.1016/j.earscirev.2023.104432

Yang, J.-W., Brandon, M., Landais, A., Duchamp-Alphonse, S., Blunier, T., Prié, F., & Extier, T. (2022). Global biosphere primary productivity changes during the past eight glacial cycles. *Science*, *375*(6585), 1145–1151. https://doi.org/10.1126/science.abj8826

Zhang, Y., Narayanappa, D., Ciais, P., Li, W., Goll, D., Vuichard, N., et al. (2022). Evaluating the vegetation–atmosphere coupling strength of ORCHIDEE land surface model (v7266). *Geoscientific Model Development*, *15*(24), 9111–9125. https://doi.org/10.5194/gmd-15-9111-2022

Erratum

The originally published version of this article contained an error. The reference for Alexandre et al., 2025 has been corrected to Alexandre, 2025, and the full reference has been corrected as follows: Alexandre, A. (2025). Climate and triple oxygen isotope of precipitation, groundwater, soil water, plant water, and phytolith data from West Africa (Benin and Senegal) [dataset bundled publication]. *PANGAEA*. https://doi.org/10.1594/PANGAEA.984133. This may be considered the authoritative version of record.